Reactions of Neutral and Cationic Diamide-Supported Imido Complexes with CO_2 and Other Heterocumulenes: Issues of Site Selectivity

Benjamin D. Ward,[†] Gavin Orde,[†] Eric Clot,*[,‡] Andrew R. Cowley,[†] Lutz H. Gade,*[,§] and Philip Mountford*[,†]

Chemistry Research Laboratory, University of Oxford, Mansfield Road, Oxford OX1 3TA, U.K., LSDSMS (UMR 5636), cc 14, Université Montpellier 2, Place Eugène Bataillon, 34095 Montpellier Cedex 5, France, and Anorganisch-Chemisches Institut, Universität Heidelberg, Im Neuenheimer Feld 270, 69120 Heidelberg, Germany

Received January 13, 2005

Experimental and DFT computational studies of the reactions of the cationic diamide-pyridine-supported methyl tungsten complex $[W(NPh)(N_2N_{py})Me]^+$ (**2**$^+$) with the heterocumulenes CO_2, CS_2, RNCO, and RNCS (R = *tert*-butyl or aryl) are described, together with comparative studies of the group 5 compounds $M(N^tBu)(N_2N_{py})Cl(py)$ (M = Nb (**13**) or Ta (**14**)) and $Ta(N^tBu)(N_2N_{py})Me$ (N_2N_{py} = $MeC(2\text{-}C_5H_4N)(CH_2NSiMe_3)_2$). In all of the reactions of **2**$^+$ the heterocumulene inserted exclusively into a $W-N_{amide}$ bond to give unstable intermediates (isolated for certain isocyanate substrates), which subsequently underwent rearrangement via a 1,3-migration of a $SiMe_3$ group. DFT studies of the reaction of **2**$^+$ with CO_2 showed that insertion into the W−Me bond is in fact thermodynamically preferred, but that insertion into $W-N_{amide}$ is kinetically more facile. Cycloaddition to the W=NPh bond was neither kinetically nor thermodynamically viable. The reactions between $Ta(N^tBu)(N_2N_{py})Me$ and CO_2 or RNCO in contrast gave complex mixtures, as did those between **13** and **14** and CO_2. DFT studies showed that in a neutral but otherwise identical tantalum analogue of **2**$^+$ the preference for substrate attack at the $M-N_{amide}$ bond is much less pronounced. Reactions of **13** and **14** with the more sterically discriminating RNCO (R = ^{t}Bu or *p*-tolyl) did, however, exclusively afford $M-N_{amide}$ insertion/1,3-$SiMe_3$ migration products, and $Nb(N^tBu)\{MeC(2\text{-}C_5H_4N)(CH_2NSiMe_3)(CH_2NC(OSiMe_3)N^tBu)\}Cl$ was structurally characterized. The previously reported reaction of $Ti(N^tBu)(N_2N_{py})(py)$ with ArNCO (Ar = 2,6-$C_6H_3{}^iPr_2$) was re-evaluated and shown to involve an analogous $Ti-N_{amide}$ insertion/1,3-$SiMe_3$ migration reaction, ultimately forming $Ti(N^tBu)\{MeC(2\text{-}C_5H_4N)(CH_2NSiMe_3)(CH_2NC(N(Ar)\text{-}SiMe_3)O)\}(py)$.

Introduction

Although transition metal imido complexes have been known since the late 1950s,[1,2] it was only during the last two decades that a particularly intense effort was made in exploring their syntheses, structures, and reactivity. Several general reviews[3−5] and a number of more specific ones are available.[6−17]

We have been interested in the chemistry of imido compounds supported by the diamido-pyridine ligand $MeC(2\text{-}C_5H_4N)(CH_2NSiMe_3)_2$ (N_2N_{py})[11,18] and have described the synthesis and reactions of such derivatives for group 4,[19−23] 5,[24,25] and 6[26,27] d^0 transition metals.

* To whom correspondence should be addressed. E-mail: clot@univ-montp2.fr.; lutz.gade@uni-hd.de; philip.mountford@chem.ox.ac.uk.
† University of Oxford.
‡ Université Montpellier 2.
§ Universität Heidelberg.

(1) Clifford, A. F.; Kobayashi, C. S. Abstracts of the 130th National Meeting, ACS, 50R, Atlantic City, NJ, 1956.
(2) Milas, N. A.; Ilipulos, M. I. *J. Am. Chem. Soc.* **1959**, *81*, 6089.
(3) Nugent, W. A.; Haymore, B. L. *Coord. Chem. Rev.* **1980**, *31*, 123.
(4) Nugent, W. A.; Mayer, J. M. *Metal−Ligand Multiple Bonds*; Wiley-Interscience: New York, 1988.
(5) Wigley, D. E. *Prog. Inorg. Chem.* **1994**, *42*, 239.
(6) Mountford, P. *Chem. Commun.* **1997**, 2127 (feature article).
(7) Romao, C. C.; Kühn, F. E.; Herrmann, W. A. *Chem. Rev.* **1997**, *97*, 3197.
(8) Danopoulos, A. A.; Green, J. C.; Hursthouse, M. B. *J. Organomet. Chem.* **1999**, *591*, 36.
(9) Cundari, T. R. *Chem. Rev.* **2000**, *100*, 807.
(10) Sharp, P. *J. Chem. Soc., Dalton Trans.* **2000**, 2647.
(11) Gade, L. H.; Mountford, P. *Coord. Chem. Rev.* **2001**, *216−217*, 65.
(12) Duncan, A. P.; Bergman, R. G. *Chem. Rec.* **2002**, *2*, 431.
(13) Eikey, R. A.; Abu-Omar, M. M. *Coord. Chem. Rev.* **2003**, *243*, 83.
(14) Leung, W.-H. *Eur. J. Inorg. Chem.* **2003**, 583.
(15) Mountford, P. In *Perspectives in Organometallic Chemistry*; Screttas, C. G., Steele, B. R., Eds.; Royal Society of Chemistry, 2003.
(16) Radius, U. *Z. Anorg. Allg. Chem.* **2004**, *630*, 957.
(17) Giesbrecht, G.; Gordon, J. C. *Dalton Trans.* **2004**, 2387.
(18) Friedrich, S.; Schubart, M.; Gade, L. H.; Scowen, I. J.; Edwards, A. J.; McPartlin, M. *Chem. Ber./Recl.* **1997**, *130*, 1751.
(19) Trösch, D. J. M.; Collier, P. E.; Bashall, A.; Gade, L. H.; McPartlin, M.; Mountford, P.; Radojevic, S. *Organometallics* **2001**, *20*, 3308.
(20) Blake, A. J.; Collier, P. E.; Gade, L. H.; Mountford, P.; Pugh, S. M.; Schubart, M.; Skinner, M. E. G.; Trösch, D. J. M. *Inorg. Chem.* **2001**, *40*, 870.
(21) Pugh, S. M.; Trösch, D. J. M.; Wilson, D. J.; Bashall, A.; Cloke, F. G. N.; Gade, L. H.; Hitchcock, P. B.; McPartlin, M.; Nixon, J. F.; Mountford, P. *Organometallics* **2000**, *19*, 3205.
(22) Bashall, A.; Collier, P. E.; Gade, L. H.; McPartlin, M.; Mountford, P.; Pugh, S. M.; Radojevic, S.; Schubart, M.; Scowen, I. J.; Trösch, D. J. M. *Organometallics* **2000**, *19*, 4784.
(23) Ward, B. D.; Maisse-François, A.; Mountford, P.; Gade, L. H. *Chem. Commun.* **2004**, 704.
(24) Pugh, S. M.; Trösch, D. J. M.; Skinner, M. E. G.; Gade, L. H.; Mountford, P. *Organometallics* **2001**, *20*, 3531.
(25) Pugh, S. M.; Blake, A. J.; Gade, L. H.; Mountford, P. *Inorg. Chem.* **2001**, *40*, 3992.

10.1021/om0500265 CCC: $30.25
Publication on Web 04/02/2005

Chart 1

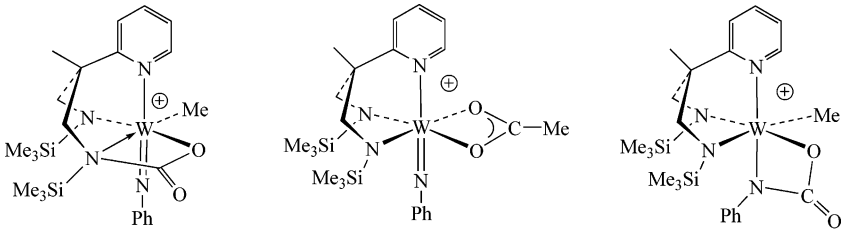

3a$^+$ **3b**$^+$ **3c**$^+$

In terms of reactivity of the M=NR bonds themselves in complexes of the type M(NR)(N_2N_{py})(L) (L = neutral or anionic co-ligand or none), only the group 4 systems Ti(NR)(N_2N_{py})(py) and certain homologues have so far been exploited (with a good degree of success).[11,19,21,23,28,29]

We very recently described the synthesis and DFT bonding analysis of the cation [W(NPh)(N_2N_{py})Me]$^+$ (**2**$^+$, valence isoelectronic with Ti(NR)(N_2N_{py})(py)), which is formed by reaction of W(NPh)(N_2N_{py})Me_2 (**1**) with BAr^F_3 or [CPh_3][BAr^F_4] (Ar^F = C_6F_5).[27] Cation **2**$^+$ undergoes facile methyl group exchange reactions with $ZnMe_2$ and Cp_2ZrMe_2, as well as with **1** itself, and we were interested in exploring its reactions with unsaturated substrates. In particular, the question of reactive site selectivity was an interesting one since all three bonds W−Me, W−N_{amide}, and W=N_{imide} might react, depending on the chosen substrates. We note in particular in this context previous studies by Legzdins et al. on some pentamethylcyclopentadienyl-supported tungsten alkylimido and -amido and related complexes and their reactions with heterocumulenes,[30,31] and work by Lam et al.[32] on the reactions of Cr(N^tBu)$_2$(NH^tBu)$_2$ with isocyanates.

In this contribution we describe the reactions of **2**$^+$ with a number of heterocumulenes and employ DFT calculations to rationalize the respective outcome and gain additional insight into these systems. Together with this work, we also report comparative studies of some group 5 analogues and a re-evaluation of the reaction of Ti(N^tBu)(N_2N_{py})(py) with ArNCO (Ar = 2,6-$C_6H_3{}^iPr_2$).

Results and Discussion

Reactions of [W(NPh)(N_2N_{py})Me][$MeBAr^F_3$] (2-$MeBAr^F_3$) with Heterocumulenes. We describe first the reactions of heterocumulenes with the in-situ-generated tungsten methyl cation [W(NPh)(N_2N_{py})Me]$^+$ (**2**$^+$), prepared as its [$MeBAr^F_3$]$^-$ salt by reaction of W(NPh)(N_2N_{py})Me_2 (**1**) with B(Ar^F)$_3$ as reported previously.[27] Compound **2-MeBAr$^F_3$** has limited stability in CH_2Cl_2 at ambient temperature (half-life of ca. 2 h), but this is not a problem from the point of view of the reactivity studies reported here since its rapid reactions with heterocumulenes are complete well before the onset of decomposition. Unfortunately the reactions of **2-MeBAr$^F_3$** with substituted allenes gave ill-defined mixtures.

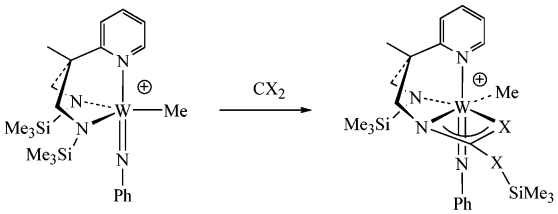

2$^+$ X = O (**3**$^+$) or S (**4**$^+$) (1)

Reaction of **2-MeBAr$^F_3$** with CO_2 (1 atm) in CH_2Cl_2 at 0 °C affords [W(NPh)(MeC(2-C_5H_4N)(CH_2NSiMe_3)-{$CH_2NCO(SiMe_3)O$}Me][$MeBAr^F_3$] (**3-MeBAr$^F_3$**, eq 1) as a golden-brown solid. The formation of **3**$^+$ is quantitative when the reaction is followed by NMR spectroscopy in CD_2Cl_2. No intermediates were observed when the reaction was carried out on an NMR tube scale in CD_2Cl_2 at −78 °C. We have been unable to grow diffraction-quality crystals of **3-MeBAr$^F_3$** or any of the cationic insertion products formed from **2-MeBAr$^F_3$** and heterocumulenes. The structures of the analytically pure and isolated tungsten products have been assigned by careful NMR analysis (employing as appropriate ^{13}C-labeled isotopomers, namely, the previously reported[27] [W(NPh)(N_2N_{py})($^{13}CH_3$)]$^+$ or/and $^{13}CO_2$) and by analogy with a crystallographically characterized, valence isoelectronic niobium analogue **15** (vide infra).

Cation **3**$^+$ appears to be formed from the insertion of CO_2 into one of the W−N_{amide} bonds of **2**$^+$ followed by a N to O $SiMe_3$ group 1,3-migration. The likely intermediate **3a**$^+$ (Chart 1) was not observed at −78 °C, but DFT evidence in support of its formation is presented later. The metal-bound Me group shows ^{183}W satellites in the ^{13}C NMR spectrum (^{183}W natural abundance = 14.5%, I = $^1/_2$; ^1J(WC) = 92 Hz), which rules out an alternative product **3b**$^+$ (or one of its coordination isomers). Only one of the chemically inequivalent $SiMe_3$ groups of **3**$^+$ shows an NOE to the rest of the compound [careful analysis of the ROESY (rotating frame nuclear Overhauser enhancement spectroscopy) spectrum established this as the N-bound $SiMe_3$ group]. Significantly the HMBC (heteronuclear multiple bond correlation) ^{1}H−^{13}C NMR spectrum clearly shows a correlation between the quaternary *C*O$SiMe_3$ carbon (δ 166.6 ppm, confirmed by use of $^{13}CO_2$) and two of the ligand "arm" methylene H atoms. This unambiguously establishes the formation of a N_{amide}−CO_2 bond as opposed to alternative coupling between CO_2 and the W=N_{imide} moiety (as in **3c**$^+$). This long-range correlation between

(26) Ward, B. D.; Dubberley, S. R.; Gade, L. H.; Mountford, P. *Inorg. Chem.* **2003**, *42*, 4961.
(27) Ward, B. D.; Orde, G.; Clot, E.; Cowley, A. R.; Gade, L. H.; Mountford, P. *Organometallics* **2004**, *23*, 4444.
(28) Blake, A. J.; Collier, P. E.; Gade, L. H.; Mountford, P. *Chem. Commun.* **1997**, 1555.
(29) Bashall, A.; Collier, P. E.; Gade, L. H.; McPartlin, M.; Mountford, P.; Troesch, D. J. M. *Chem. Commun.* **1998**, 2555.
(30) Legzdins, P.; Phillips, E. C.; Rettig, S. J.; Trotter, J.; Veltheer, J. E.; Yee, V. C. *Organometallics* **1992**, *11*, 3104.
(31) Legzdins, P.; Rettig, S. J.; Ross, K. J. *Organometallics* **1994**, *13*, 569.
(32) Lam, H. W.; Wilkinson, G.; Hussain-Bates, B.; Hursthouse, M. B. *J. Chem. Soc., Dalton Trans.* **1993**, 781.

Scheme 1

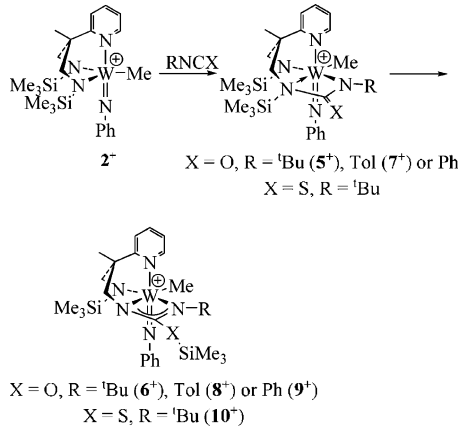

methylene H atoms and the quaternary carbon originating from the heterocumulene is a common feature of all of the new $M-N_{amide}$ insertion products reported herein (including the crystallographically characterized **15**). CS_2 undergoes an analogous reaction with $\mathbf{2}^+$ to form $\mathbf{4}^+$ (eq 1), this time involving an N to S $SiMe_3$ 1,3-migration.

The reaction of **2-MeBAr$^F_3$** with *tert*-butyl, *p*-tolyl, or phenyl isocyanates, or with *tert*-butyl isothiocyanate, afforded products analogous to **3-MeBAr$^F_3$** and **4-MeBAr$^F_3$**, namely, [W(NPh)(MeC(2-C_5H_4N)(CH_2NSiMe_3)-{$CH_2NCO(SiMe_3)NR$}Me][$MeBAr^F_3$] (R = tBu (**6-MeBAr$^F_3$**), Tol (Tol = 4-C_6H_4Me, **8-MeBAr$^F_3$**), or Ph (**9-MeBAr$^F_3$**)) or [W(NPh)(MeC(2-C_5H_4N)(CH_2NSiMe_3)-{$CH_2NCS(SiMe_3)N^tBu$}Me][$MeBAr^F_3$] (**10-MeBAr$^F_3$**), respectively (Scheme 1). The NMR data are consistent with the heterocumulene having inserted into one of the $W-N_{amide}$ bonds of $\mathbf{2}^+$ with the subsequent migration of a $SiMe_3$ group, as proposed for the reaction with CO_2 and CS_2. The non-centrosymmetric heterocumulenes can insert into a $W-N_{amide}$ bond of $\mathbf{2}^+$ with either the N or O (or S for tBuNCS) bound to W. The ROESY spectra for cations $\mathbf{6}^+$ and $\mathbf{8}^+-\mathbf{10}^+$ show a clear NOE between the pyridyl H^6 atom (i.e., *ortho* to N) and H atoms of the R group originating from the heterocumulene, therefore confirming the geometries proposed in Scheme 1. As for $\mathbf{3}^+$ and $\mathbf{4}^+$ only one of the two inequivalent $SiMe_3$ groups shows NOE interactions with other parts of the cation.

Unlike the reactions of **2-MeBAr$^F_3$** with CO_2 and CS_2, reaction intermediates were observed in the heterocumulene reactions, and these have been analyzed in detail for *tert*-butyl and tolyl isocyanate (Scheme 1). The cations [W(NPh)(MeC(2-C_5H_4N)(CH_2NSiMe_3){$CH_2N(SiMe_3)$-C(O)NR}Me]$^+$ (R = tBu ($\mathbf{5}^+$) or Tol ($\mathbf{7}^+$)) were readily observed when the reactions were carried out in an NMR tube at −78 °C (CD_2Cl_2). Compound **7-MeBAr$^F_3$** was insufficiently stable to be isolated in the absence of significant amounts of the migration product **8-MeBAr$^F_3$** and was analyzed only by NMR. However, compound **5-MeBAr$^F_3$** could be isolated by carrying out the synthesis and workup at temperatures below −30 °C. The NMR data show that these compounds are the product of insertion into one of the $W-N_{amide}$ bonds of $\mathbf{2}^+$. For example, for $\mathbf{5}^+$ long-range coupling was observed between two methylene H atoms and the quaternary carbon (δ 157.5 ppm) originating from tBuNCO; both $SiMe_3$ groups showed NOE interactions to the rest

Scheme 2

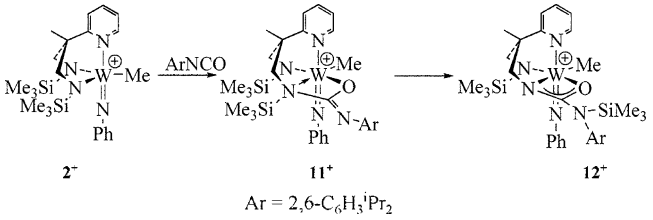

Table 1. Rate Constants and Activation Parameters for the Conversion of $\mathbf{11}^+$ into $\mathbf{12}^+$

Rate Constants

temp (K)	rate constant (s^{-1})
293	1.94×10^{-4}
298	2.32×10^{-4}
303	3.64×10^{-4}
308	3.81×10^{-4}
313	7.20×10^{-4}

Activation Parameters

$\Delta H^‡$ (kJ·mol^{-1})	$\Delta S^‡$ (J·K^{-1}·mol^{-1})	$\Delta G^‡_{298}$ (kJ·mol^{-1})
44.9 ± 2.0	−164 ± 10	93.8 ± 5

of the molecule; the tBu group shows a clear ^1H NOE to the pyridyl H^6.

Reaction of **2-MeBAr$^F_3$** with the sterically more demanding isocyanate ArNCO (Ar = 2,6-$C_6H_3{}^iPr_2$) affords a longer-lived intermediate compound [W(NPh)-(MeC(2-C_5H_4N)(CH_2NSiMe_3)($CH_2N(SiMe_3)C(NAr)O$)-Me][$MeBAr^F_3$] (**11-MeBAr$^F_3$**), in which the isocyanate has undergone $W-N_{amide}$ bond insertion with the isocyanate O atom bound to W. The intermediate cation $\mathbf{11}^+$ transforms to the silyl-migrated species [W(NPh)-(MeC(2-C_5H_4N)(CH_2NSiMe_3)($CH_2NC\{N(SiMe_3)Ar\}O$]$^+$ ($\mathbf{12}^+$) over ca. 4 h in CD_2Cl_2 at ambient temperature (Scheme 2). The NMR data for cations $\mathbf{11}^+$ and $\mathbf{12}^+$ are consistent with isocyanate insertion into a $W-N_{amide}$ bond. However, the ROESY experiments show that the isocyanate-derived aryl group is close to one of the N_2N_{py} methylene groups and one $SiMe_3$ group, but is not near the pyridyl moiety. The IR spectrum of **11-MeBAr$^F_3$** exhibits a band at 1690 cm^{-1}, which we attribute to ν(C═N), and this band is absent in the IR spectrum of **12-MeBAr$^F_3$**. We propose that the O-bound isomer is formed in this case due to the increased steric demand imposed by the 2,6-$C_6H_3{}^iPr$ group. The slower isomerization rate of cation $\mathbf{11}^+$ compared to $\mathbf{5}^+$ and $\mathbf{7}^+$ can be attributed (at least in part) to the $SiMe_3$ migrating to a substituted acceptor atom in the case of $\mathbf{11}^+$.

The transformation of cation $\mathbf{11}^+$ into $\mathbf{12}^+$ was monitored by ^1H NMR spectroscopy at five temperatures between 293 and 313 K. The decay of $\mathbf{11}^+$ and evolution of $\mathbf{12}^+$ followed first-order kinetics (see the SI for further details), and the rate constants are given in Table 1, together with associated activation parameters. The very negative $\Delta S^‡$ and first-order kinetics strongly indicate a highly concerted, intramolecular process, most likey involving a transition state featuring a hypervalent Si atom bridging the originating N_{amide} atom and the acceptor N atom (or O or S for the reactions in Scheme 1 and eq 1). 1,3-$SiMe_3$ shifts between various types of donor and acceptor atoms have been well characterized in a number of organic[33] and inorganic[34−36] systems.

(33) Kwart, H.; Barnette, W. E. *J. Am. Chem. Soc.* **1977**, *99*, 614.

Reactions of M(N^{t}Bu)(N$_2$N$_{py}$)Cl(py) (M = Nb or Ta) with Heterocumulenes. The methyl tungsten cation [W(NPh)(N$_2$N$_{py}$)Me]$^+$ (**2**$^+$) evidently shows a strong preference (at least kinetically) for insertion of heterocumulenes into a W−N$_{amide}$ bond as opposed to cycloaddition to W=NPh or insertion into W−Me. We were therefore interested in examining the corresponding reactions of neutral group 5 analogues. We have previously reported the chloride compounds M(N^{t}Bu)(N$_2$N$_{py}$)Cl(py) (M = Nb (**13**) or Ta (**14**)).[25] These are in dynamic equilibrium with the five-coordinate M(N^{t}Bu)(N$_2$N$_{py}$)Cl (valence isoelectronic with **2**$^+$) and pyridine on the NMR time scale.[25] The pyridine-free niobium compound Nb(N^{t}Bu)(N$_2$N$_{py}$)Cl has been isolated and characterized but is much less stable than the six-coordinate **13**. The tantalum compound **14** is cleanly methylated to form Ta(N^{t}Bu)(N$_2$N$_{py}$)Me,[27] again valence isoelectronic with **2**$^+$, whereas the congeneric **13** cannot be successfully methylated.[24] Although group 5 *tert*-butyl imido compounds **13** and **14** could be readily made, phenyl imido homologues were not accessible.[27,37] Our group 5 work has therefore concentrated on reactions of M(N^{t}Bu)(N$_2$N$_{py}$)Cl(py) and Ta(N^{t}Bu)(N$_2$N$_{py}$)Me.

The reactions of M(N^{t}Bu)(N$_2$N$_{py}$)Cl(py) and Ta(N^{t}Bu)(N$_2$N$_{py}$)Me are much less well-behaved than those of **2-MeBAr^F$_3$**. Briefly, reactions of Ta(N^{t}Bu)(N$_2$N$_{py}$)Me with CO_2, TolNCO, ^{t}BuNCO, or ArNCO all gave complex mixtures of products. Reaction of **13** or **14** with CO_2 also gave complex mixtures, although in these instances ^{t}BuNCO was apparent in NMR tube scale reactions (formed in 30−40% yield based on **13** and **14** starting complexes). The ^{t}BuNCO is most likely formed by cycloaddition to M=N^{t}Bu followed by extrusion (cycloreversion), which is a well-established reaction sequence in transition metal imido chemistry.[38] However, the low yield of ^{t}BuNCO and complex mixture formed suggests that other modes of reaction are easily accessible.

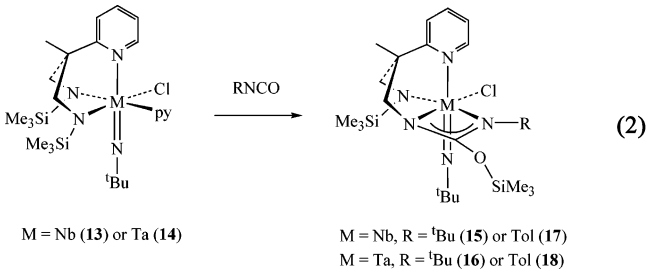

(2)

However, despite these discouraging results, compounds **13** and **14** do undergo very clean reactions with ^{t}BuNCO and TolNCO to form the corresponding products M(N^{t}Bu){MeC(2-C$_5$H$_4$N)(CH$_2$NSiMe$_3$)(CH$_2$NC(OSiMe$_3$)NR)}Cl) (M = Nb, R = ^{t}Bu (**15**) or Tol (**17**); M = Ta, R = ^{t}Bu (**16**) or Tol (**18**)) (eq 2). These are neutral analogues of the cations **6**$^+$ and **8**$^+$ (eq 1) and again possess 1,3-migrated SiMe$_3$ groups. The isocyanates have reacted in such a way that the N atoms are bound to the metal. The NMR data are consistent with the proposed structures in the same manner as described above for the cationic tungsten systems. Furthermore the niobium compound **15** has been structurally characterized. Crystals of **15** contain four independent molecules in the asymmetric unit. There are no substantial differences between them. The molecular structure of one of the crystallographically independent molecules is shown in Figure 1, and selected bond distances and angles are listed in Table 2.

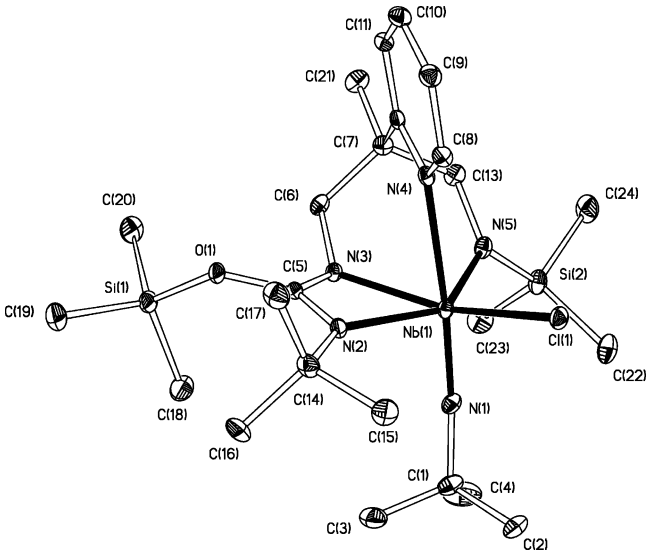

Figure 1. Displacement ellipsoid plot (20%) of one of the four crystallographically independent molecules of Nb(N^{t}Bu){MeC(2-C$_5$H$_4$N)(CH$_2$NSiMe$_3$)(CH$_2$NC(OSiMe$_3$)N^{t}Bu)}Cl (**15**). H atoms are omitted for clarity.

The structure of **15** confirms the presence of a 1,3-migrated SiMe$_3$ group and the presence of a new bond formed between Nb−N$_{amide}$ and the carbon of ^{t}BuNCO. In general the distances and angles are in agreement with previously reported values.[39,40] The starting compound M(N^{t}Bu)(N$_2$N$_{py}$)Cl(py) (**13**) has been structurally characterized previously.[25] The Nb(1)−N(1), Nb(1)−N(4), and Nb(1)−N(5) distances are similar in both molecules, whereas Nb(1)−Cl(1) is somewhat longer in **13** (2.548(2) Å) than in **15** (range 2.4488(13)−2.4575(13) Å). This reflects the different nature of the N atom *trans* to the Nb−Cl bond (N$_{amide}$ of N$_2$N$_{py}$ in **13** vs N(3) in **15**) and that the Nb(1)−N(3) distance in **15** (range 2.148(4)−2.150(4) Å) is ca. 0.01 Å longer than the equivalent bond in **13**, clearly refecting the modification that this part of the molecule has undergone. The {O(1)C(5)N(3)N(2)} moiety in **15** posesses a trigonal planar geometry at C(5) and forms the core of a formally monoanionic O-silylated ureate fragment. Comparison of the C(5)−N(2) and C(5)−N(3) distances suggests there is greater multiple bond character in the former bond. Consistent with the greater implied imino character of N(2), the Nb(1)−N(2) distances are ca. 0.12−0.14 Å longer than the Nb(1)−N(3) values (thus N(3) appears to have more residual N$_{amide}$ character).

Re-evaluation of the Reaction of Ti(N^{t}Bu)(N$_2$N$_{py}$)(py) with ArNCO. The Ti=N^{t}Bu bond in Ti(N^{t}Bu)(N$_2$N$_{py}$)(py) undergoes a wide range of cycloaddition and other coupling reactions with unsaturated substrates.[19−23] The reaction with allene itself affords crystallographically characterized **19** (Chart 2).[19] Reactions with a range of isocyanates and CO_2 all gave multiple products except in the case of the bulky ArNCO (Ar = 2,6-C$_6$H$_3$^{i}Pr$_2$), which formed a rather thermally unstable product, which was assigned the structure **20a** (Chart 2) on the basis of available NMR data (300 MHz ^{1}H frequency) at the time. In light of the new results described above for Nb, Ta, and W imido compounds supported by N$_2$N$_{py}$ the structure **20a** appeared questionable, and we have

Table 2. Selected Bond Lengths (Å) and Angles (deg) for Nb(N^{t}Bu){MeC(2-C$_5$H$_4$N)(CH$_2$NSiMe$_3$)(CH$_2$NC(OSiMe$_3$)N^{t}Bu)}Cl (15)[a]

Nb(1)−N(1)	1.771(4)	[1.774(4)]	[1.776(4)]	[1.776(4)]
Nb(1)−N(2)	2.267(4)	[2.280(4)]	[2.281(4)]	[2.287(4)]
Nb(1)−N(3)	2.148(4)	[2.150(4)]	[2.149(4)]	[2.148(4)]
Nb(1)−N(4)	2.468(4)	[2.449(4)]	[2.453(4)]	[2.447(4)]
Nb(1)−N(5)	2.006(4)	[2.006(4)]	[2.010(4)]	[2.008(4)]
Nb(1)−Cl(1)	2.4488(13)	[2.4531(14)]	[2.4492(14)]	[2.4575(13)]
C(5)−N(2)	1.302(6)	[1.296(6)]	[1.299(7)]	[1.308(6)]
C(5)−N(3)	1.335(6)	[1.334(6)]	[1.344(7)]	[1.330(6)]
Cl(1)−Nb(1)−N(1)	97.09(14)	[95.83(15)]	[96.78(15)]	[93.84(13)]
Cl(1)−Nb(1)−N(2)	100.29(11)	[101.61(11)]	[100.43(11)]	[101.84(11)]
N(1)−Nb(1)−N(2)	97.00(18)	[97.02(17)]	[95.59(18)]	[97.43(17)]
Cl(1)−Nb(1)−N(3)	152.10(11)	[153.66(12)]	[153.76(12)]	[154.66(12)]
N(1)−Nb(1)−N(3)	104.12(18)	[104.02(18)]	[101.95(18)]	[104.87(17)]
N(2)−Nb(1)−N(3)	59.66(15)	[59.31(15)]	[59.82(16)]	[59.43(15)]
Cl(1)−Nb(1)−N(4)	83.13(9)	[82.97(11)]	[84.2(1)]	[83.15(11)]
N(1)−Nb(1)−N(4)	173.87(17)	[173.40(18)]	[172.80(17)]	[173.42(17)]
N(2)−Nb(1)−N(4)	76.96(14)	[76.93(15)]	[77.23(14)]	[77.56(14)]
N(3)−Nb(1)−N(4)	73.86(14)	[75.32(15)]	[75.03(15)]	[76.40(15)]
Cl(1)−Nb(1)−N(5)	106.03(13)	[106.58(13)]	[105.80(13)]	[107.38(13)]
N(1)−Nb(1)−N(5)	103.95(19)	[104.00(19)]	[105.36(19)]	[104.17(18)]
N(2)−Nb(1)−N(5)	143.71(16)	[142.55(16)]	[143.88(17)]	[142.02(16)]
N(3)−Nb(1)−N(5)	86.39(16)	[85.43(16)]	[86.86(18)]	[84.76(16)]
N(4)−Nb(1)−N(5)	81.81(16)	[82.54(16)]	[81.16(15)]	[82.34(15)]
Nb(1)−N(1)−C(10	168.0(4)	[168.6(4)]	[168.1(4)]	[166.7(4)]

[a] The values in brackets refer to the other crystallographically independent molecules in the asymmetric unit.

Chart 2

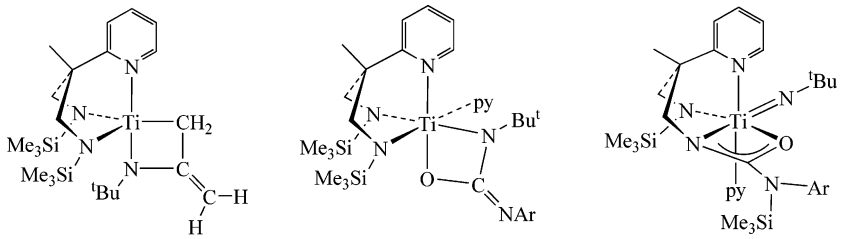

19 **20a** **20b**

therefore re-evaluated the reaction of Ti(N^{t}Bu)(N$_2$N$_{py}$)(py) with ArNCO. Careful re-examination of the NMR data (in particular the high-field ROESY and HMBC spectra which were not available to us at the time of the previous studies) have allowed us to reassign the structure as **20b** (Chart 2). Thus d^0 **20b** and **12**$^+$ are valence isoelectronic with two structural differences: the imido ligand in **12**$^+$ is *trans* to the pyridyl donor, whereas in **20b** it is *cis*; in **12**$^+$ the migrated SiMe$_3$ group lies toward the "front" of the complex (i.e., proximal to the pyridyl H^6 atom), whereas in **20b** the SiMe$_3$ lies more toward the "rear" according to the ROESY spectra.

Computed Reaction Mechanism with CO$_2$. In the next part of this contribution we describe a detailed DFT study of the reactions of the group 5 and 6 diamide-supported imido compounds with CO$_2$ and isocyanates. The bonding in imido compounds in general is well understood, especially with regard to aspects of their ground state electronic structures.[9,27] However, there have been relatively few computational (and in particular DFT) studies of the reactions of imido complexes described to date in which reaction site selectivity has been explored.[41]

The reaction between the cation [W(NPh)(N$_2$N$_{py}$)Me]$^+$ (**2**$^+$) and CO$_2$ can potentially occur at three different sites: the W=N$_{imide}$, the W−Me, and the W−N$_{amide}$ bonds (Chart 1, Scheme 3). As CO$_2$ is a poor ligand, the main interaction expected upon reaction of CO$_2$ with **2**$^+$ is a donation from an occupied MO of the complex into the LUMO of CO$_2$. The shape and energy of the occupied frontier orbitals of **2**$^+$ are thus indicative of the potential reactivity of the latter with CO$_2$. We have previously shown that the two highest occupied MOs of **2**$^+$ are essentially nonbonding combinations of the N$_{amide}$ lone pairs lying in the W−Me bonding equatorial plane.[27] The π-bonding MOs of the W=N$_{imide}$ linkage are at significantly lower energy. It is thus expected that the preferred kinetic reaction between **2**$^+$ and CO$_2$ is the insertion at a W−N$_{amide}$ or W−Me bond. In reality, insertion into the W−N$_{amide}$ occurs exclusively, followed by a 1,3-SiMe$_3$ migration.

(34) Campion, B. K.; Heyn, R. H.; Tilley, T. D. *Organometallics* **1993**, *12*, 2584.
(35) Gerlach, C. P.; Arnold, J. *Inorg. Chem.* **1996**, *35*, 5770.
(36) Cole, M. L.; Junk, P. C. *Dalton Trans.* **2003**, 2109.
(37) Orde, G. Part II Thesis: Honours School of Natural Science: Chemistry; University of Oxford, 2003.
(38) See for example: Guiducci, A. E.; Cowley, A. R.; Skinner, M. E. G.; Mountford, P. *J. Chem. Soc., Dalton Trans.* **2001**, 1392.
(39) Allen, F. H.; Kennard, O. *Chem. Des. Autom. News* **1993**, *8*, 1 & 31.
(40) Fletcher, D. A.; McMeeking, R. F.; Parkin, D. J. *Chem. Inf. Comput. Sci.* **1996**, *36*, 746.
(41) (a) Jensen, V. R.; Borve, K. J. *Chem. Commun.* **2002**, 542. (b) Jensen, V. R.; Borve, K. J. *Organometallics* **2001**, *20*, 616. (c) Monteyne, K.; Ziegler, T. *Organometallics* **1998**, *17*, 5901.

Scheme 3. Schematic Representation of the Three Different Insertion Reactions Possible between 2^+ and CO_2: Insertion into the W−N_{amide} Bond (AmInt), Insertion into the W−Me Bond (MeProd), and Cycloaddition to the W=N_{imide} π-Bond (ImProd)[a]

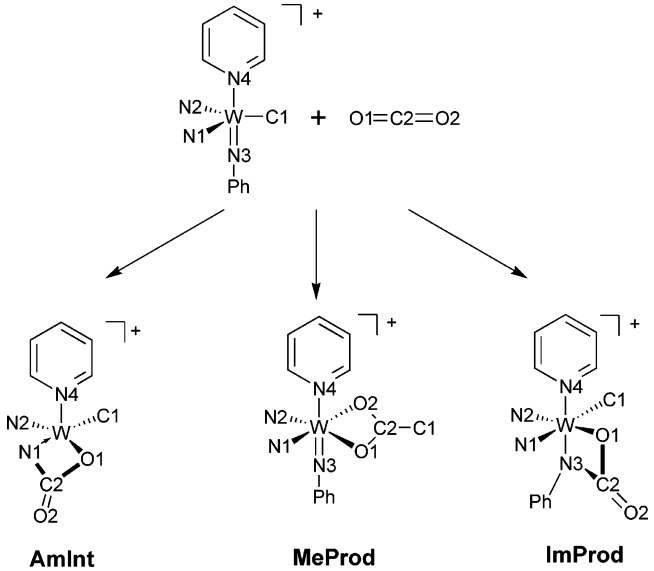

[a] The numbering scheme shown will be used systematically in the theoretical study. For the clarity of the representation, the group N3−Ph has been omitted in **AmInt**.

To study in more detail these competitive pathways, DFT(B3PW91) and ONIOM(B3PW91:UFF) calculations have been carried out. In the DFT calculations the ligand N_2N_{py} has been modeled by HC(2-C_5H_4N)(CH_2-$NSiH_3$)$_2$ (abbreviated as N_2N_{qm}), and the missing Me groups have been treated at the MM level (UFF) in the ONIOM calculations. The QM part of the ONIOM calculations is the same as that for the DFT-only calculations. CO_2 has been explicitly treated at the DFT level in all calculations.

Electronic Effects: B3PW91 Calculations. The cation [W(NPh)(N_2N_{qm})(Me)]$^+$ (**2_{qm}**) can react at three different sites with CO_2 (Scheme 3), and the corresponding transition states have been located on the potential energy surface (PES) and are shown in Figure 2. The energies (with $\Delta_r G$ values in parentheses) are expressed (kJ·mol^{-1}) with respect to the separated reactants **2_{qm}** and CO_2. Table S1 in the Supporting Information lists some selected geometric parameters for the three TS structures and also for **2_{qm}** as a reference.

The transition state (TS) corresponding to the insertion into the W−N_{amide} bond, **AmTS1$_{qm}$**, is at a significantly lower energy than the two other TS structures (31.5 kJ·mol^{-1} for **AmTS1$_{qm}$** vs 88.8 and 106.6 kJ·mol^{-1} for **MeTS$_{qm}$** and **ImTS$_{qm}$**, respectively) and is therefore associated with the preferred pathway, in excellent agreement with the experimental results and the qualitative frontier MO analysis.

The insertion into the W−N_{amide} bond is easier than insertion into the W−Me bond or cycloaddition at the W=N_{imide} bond because less structural reorganization is necessary to accommodate the incoming ligand. The N1−W−C1 angle (numbering for the atoms is shown in Scheme 3) opens up by ca. 30° (121.9° in **2_{qm}** vs 149.2° in **AmTS1$_{qm}$**), but the Me group is not strictly *trans* to N1 and the W−C1 bond only slightly lengthens (2.161 Å in **2_{qm}** vs 2.180 Å in **AmTS1$_{qm}$**). The W=N_{imide} linkage is unaffected, and so the stabilizing influence through π-donation from N3 to W is maintained in **AmTS1$_{qm}$**. Furthermore, the transition state structure is relatively early on the pathway to the product, as illustrated by the long W···O1 (2.347 Å) and C2···N1 (2.226 Å) distances. This is due to the shape of the HOMO of **2_{qm}**, effectively a nonbonding lone pair on N1 ready to interact with CO_2. Because of the nonbonding character of this lone pair, no large destabilization occurs when the W−N1 bond is elongated from 1.928 Å in **2_{qm}** to 2.075 Å in **AmTS1$_{qm}$** to accommodate the CO_2 insertion.

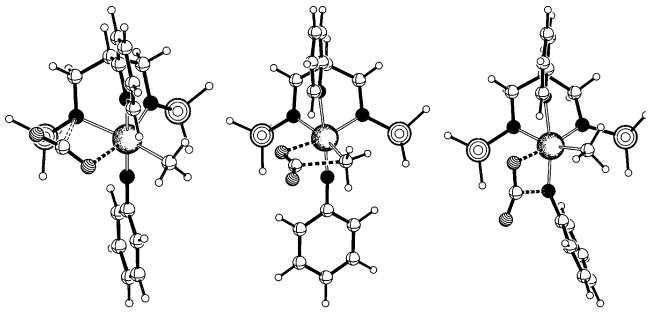

Figure 2. Optimized geometry (B3PW91) for the three transition states associated with the three different insertion/cycloaddition reactions of CO_2 with **2_{qm}**. Energy values (Gibbs free energy values in parentheses) are given relative to separated reactants **2_{qm}** and CO_2 in kJ·mol^{-1}.

The situation is rather different for the insertion into the W−Me bond (**MeTS$_{qm}$** in Figure 2). Here the W−C1 bond is significantly elongated (2.161 Å in **2_{qm}** vs 2.343 Å in **MeTS$_{qm}$**), and to achieve better overlap with the LUMO of CO_2, the C1···C2 distance has to be short and the CH_3 group must be tilted to put the "sp^3 lone pair" in the proper direction for interaction. The π-donation from the imido and amido ligands is preserved in **MeTS$_{qm}$** (see geometric parameters in Table S1), and the destabilization is mainly associated with the stretching of the W−Me bond to achieve insertion.

Finally, the least preferred pathway corresponds to cycloaddition to the W=NPh bond with a higher energy barrier to overcome (Figure 2). We have shown[27] that the geometry of 2^+ results from a subtle interplay between π-donating properties of the ligands and steric repulsion between the ligands. The electronic preference is to have the good π-donor imido ligand *trans* to pyridyl, and therefore the associated π-bond bonding MOs are rather low-lying and less available for reaction. This explains the high energy barrier associated with the cycloaddition and is reflected by some important geometric changes in **ImTS$_{qm}$** (see Table S1). Most noticeably, one π-bond to W is lost, as illustrated by the lengthening of W−N3 (1.747 Å in **2_{qm}** vs 1.823 Å in **ImTS$_{qm}$**) and the tilting of the imido substituent (W−N3−Ph = 150.7° in **ImTS$_{qm}$**). Also the C2···N3 distance in **ImTS$_{qm}$** is much shorter than the corresponding one (C2···N1) in **AmTS1$_{qm}$** (1.892 vs 2.226 Å) to achieve better overlap.

The products for the three reactions are shown in Figure 3 along with their relative energies with respect

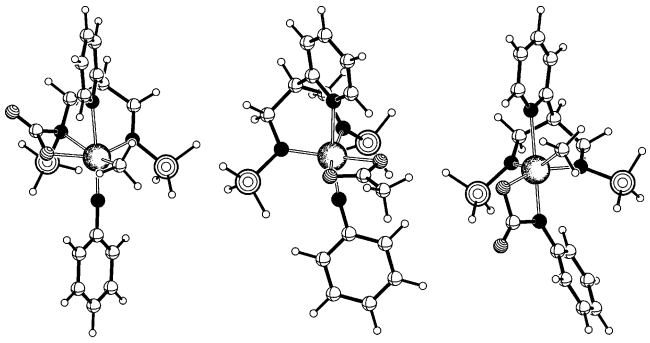

Figure 3. Optimized geometry (B3PW91) for the three products associated with the three different insertion reactions of CO_2 with $\mathbf{2_{qm}}$. Energy values (Gibbs free energy values in parentheses) are given relative to separated reactants $\mathbf{2_{qm}}$ and CO_2 in kJ·mol^{-1}.

to the reactants. A comprehensive listing of geometric parameters is given in Table S1 in the SI. The cycloaddition reaction giving $\mathbf{ImProd_{qm}}$ is very endothermic ($\Delta_r G$ = +123.7 kJ·mol^{-1}), and this product is very unlikely to be formed. The high energy of $\mathbf{ImProd_{qm}}$ results from the loss of π-donation from N3, as this atom is now involved in the metallacycle. This is illustrated by the lengthening of W−N3 (1.747 Å in $\mathbf{2_{qm}}$ vs 2.002 Å in $\mathbf{ImProd_{qm}}$) and the tilting of the phenyl group attached to N3 (168.7° in $\mathbf{2_{qm}}$ vs 140.9° in $\mathbf{ImProd_{qm}}$). The Me ligand is also significantly out of the equatorial plane with a slightly longer W−C1 bond, which could also contribute to the high energy of $\mathbf{ImProd_{qm}}$.

The insertion reaction into the W−Me bond is very exothermic ($\Delta_r G$ = −94.8 kJ·mol^{-1}) and leads to the η^2-acetato complex $\mathbf{MeProd_{qm}}$ (Figure 3). From $\mathbf{MeTS_{qm}}$ we were not able to locate any intermediate (e.g., an η^1-acetato) and $\mathbf{MeProd_{qm}}$ was the only structure obtained. The thermodynamic stability of $\mathbf{MeProd_{qm}}$ is due to the ligand environment with six hard π-donor ligands attached to the hard d^0 W^{VI} center. However, the kinetic barrier to form $\mathbf{MeProd_{qm}}$ is too high ($\Delta_r G^{\#}$ = +137.5 kJ·mol^{-1}) and, also, another lower energy pathway is available. This explains why, despite its thermodynamic stability, $\mathbf{MeProd_{qm}}$ is not observed experimentally.

CO_2 insertion into the W−N_{amide} bond is slightly endothermic ($\Delta_r G$ = +9.6 kJ·mol^{-1}) and leads to the complex $\mathbf{AmInt_{qm}}$ (Figure 3). In the absence of unfavorable entropy contributions, the reaction is actually favored (ΔE = −51.8 kJ·mol^{-1}). However, the steric strain introduced in the modified N_2N_{qm} ligand by the formation of the four-membered ring and also the lengthening of W−N1 associated with the new sp^3 hybridization of the nitrogen atom N1 mitigate against as large a stabilization as in $\mathbf{MeProd_{qm}}$. Consequently, the thermodynamic instability of $\mathbf{AmInt_{qm}}$ is entropically driven with a $-T\Delta_r S$ value of ca. +60 kJ·mol^{-1} at 298 K (we assume that the E and H values are close).[42] Usually, for a coupling reaction between two molecules,

(42) The computed $\Delta H^{\#}$ and ΔH values were 31.8 and −45.1 kJ mol for $\mathbf{AmTS1_{qm}}$ and $\mathbf{AmInt_{qm}}$, respectively. See http://www.gaussian.com/g_whitepap/thermo/thermo.pdf for details about thermochemistry calculations within Gaussian.

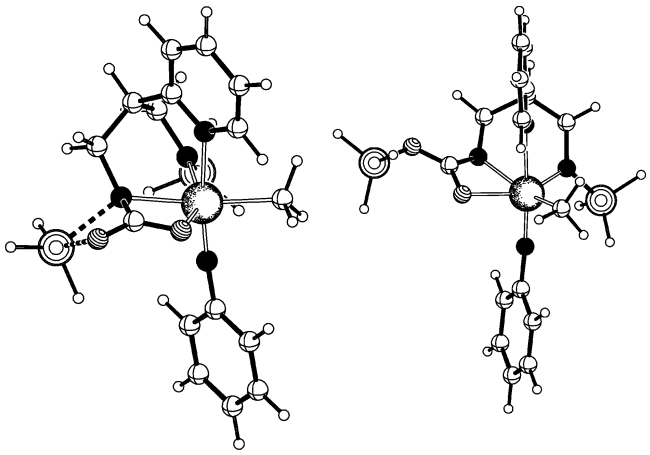

Figure 4. Optimized geometry (B3PW91) for the transition state and the product associated with the migration of SiH_3 from N to O. Energy values (Gibbs free energy values in parentheses) are given relative to separated reactants $\mathbf{2_{qm}}$ and CO_2 in kJ·mol^{-1}.

the principal contribution to the $-T\Delta_r S$ value stems from the loss of translational degrees of freedom and amounts to ca. 40 kJ·mol^{-1} at 298 K.[43] In the present case, upon formation of the four-membered ring, some rotational degrees of freedom of CO_2 are lost and these modes have large entropy contributions. The same observation holds for $\mathbf{ImProd_{qm}}$, where the $-T\Delta_r S$ value is also close to +60 kJ·mol^{-1} at 298 K (Figure 3).

The complex $\mathbf{AmInt_{qm}}$ is less stable than the reactants by ca. 10 kJ·mol^{-1} and would therefore be present in trace amounts (less than 2%), explaining why the proposed real intermediate $\mathbf{3a}^+$ (Chart 1) is not observed experimentally. However, this complex can rearrange to a more stable complex, $\mathbf{AmProd_{qm}}$, via a 1,3-migration of the SiH_3 group from N1 to O2, as illustrated by the transition state $\mathbf{AmTS2_{qm}}$ (Figure 4). The activation barrier of 105.6 kJ·mol^{-1} ($\Delta_r G^{\#}$ = 102.2 kJ·mol^{-1}) results from the bridging position of SiH_3 in $\mathbf{AmTS2_{qm}}$ with two bond distances of intermediate values (Si1−N1 = 2.182 Å and Si1−O2 = 2.059 Å; for further details see Table S2 in the SI). The O2 atom slightly moves out of the plane of the four-membered ring (W−N1−C2−O1) to achieve better interaction with Si1 in the transition state (dihedral angle N1−C2−O1−O2 = 164°). In terms of formal hybridization, N1 changes from an sp^3 amine function in $\mathbf{AmInt_{qm}}$ to an sp^2 imine/amide one in $\mathbf{AmProd_{qm}}$. Consequently, the N1−C2 bond distance shortens from the value for a single bond in $\mathbf{AmInt_{qm}}$ (1.483 Å) to that with an increased double-bond character in $\mathbf{AmProd_{qm}}$ (1.318 Å). We have also searched for a concerted pathway leading directly from $\mathbf{2_{qm}}$ to $\mathbf{AmProd_{qm}}$ through a transition state structure with a semichair conformation, as represented schematically below, but all our attempts have failed and, in every case, the TS obtained was $\mathbf{AmTS1_{qm}}$.

(43) Watson, L. A.; Eisenstein, O. *J. Chem. Educ.* **2002**, *79*, 1269.

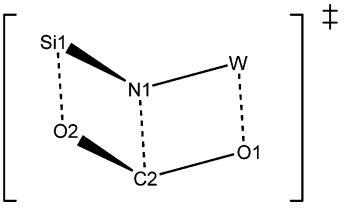

Steric Effects: ONIOM(B3PW91:UFF) Calculations. The DFT study has allowed the identification of the preferred reaction pathway as the two-step process of CO_2 insertion into the $W-N_{amide}$ bond, followed by N to O $SiMe_3$ migration (Figure 5). We have already shown that the electronic structure of $\mathbf{2}^+$ and related systems is influenced by the steric demand of the ligands in a very subtle way.[27] It was thus important to check if the steric interactions in the real system could alter the relative positions of the various reaction pathways. To this end we have performed ONIOM(B3PW91:UFF) calculations on the experimental system where the QM part was the same as in the DFT study and the "missing" Me groups ($SiMe_3$ and Me attached to bridging C in N_2N_{py}) were treated at the MM level (UFF). The ONIOM energies (kJ·mol^{-1}, evaluated from separated reactants) are given in brackets in Figure 5 for a direct comparison with the results of the B3PW91 study. Interestingly, despite many attempts, we were not able to locate at the ONIOM level a transition state structure for the CO_2 cycloaddition to W=NPh. We always observed dissociation of CO_2. The reaction at the $W=N_{imide}$ linkage is thus highly disfavored on both electronic and steric grounds.

Overall, the picture provided by the ONIOM calculations is the same as that obtained with the DFT study. The preferred pathway remains the insertion into the $W-N_{amide}$ bond followed by a 1,3-$SiMe_3$ migration. Due to the steric repulsions, all the extrema located at the ONIOM level are destabilized with respect to separated reactants when compared to the extrema at the DFT level. The insertion products $\mathbf{MeProd_{oniom}}$ and $\mathbf{AmProd_{oniom}}$ are only slightly destabilized (ca. 5 kJ·mol^{-1}, Figure 5) because the bulky ligands are either far from the site of reaction ($\mathbf{MeProd_{oniom}}$) or pushed away from the metal center ($\mathbf{AmProd_{oniom}}$). When CO_2 is closer to the $SiMe_3$ groups, then the destabilization is larger, as illustrated by the 15−25 kJ·mol^{-1} energy increase for $\mathbf{AmInt_{oniom}}$, $\mathbf{ImProd_{oniom}}$, $\mathbf{MeTS_{oniom}}$, and $\mathbf{AmTS2_{oniom}}$.

The transition state associated with the $SiMe_3$ migration, $\mathbf{AmTS2_{oniom}}$, is destabilized by more than 25 kJ·mol^{-1} (with respect to the DFT value) when the steric bulk is introduced. We suspected that the electronic influence of the migrating $SiMe_3$ group could be a factor to consider more carefully in the reaction pathway leading to the observed product. In fact, in all calculations (DFT and ONIOM) the SiR_3 groups (DFT, R = H; ONIOM R = Me) were modeled by SiH_3 in the QM calculations. To test the electronic influence of the precise nature of R, the reaction pathway leading to **AmProd** was computed at the ONIOM(B3PW91:UFF) level but with the migrating $SiMe_3$ entirely considered in the QM part (the other $SiMe_3$ being kept as SiH_3 in the QM part).

Key geometric parameters for the transition states optimized at the ONIOM level for the migration of $SiMe_3$ are shown in Table S2 of the SI for a comparison with the DFT values ($\mathbf{AmTS2_{oniom}}$, SiH_3 in QM part; $\mathbf{AmTS2_{ONIOM}}$, $SiMe_3$ in QM part). A direct comparison of the energies associated with the preferred pathway obtained with the different methods is given in Table 3. When no significant Si···O interaction is present (i.e., in **AmTS1** and **AmInt**), the results are similar whatever the method used. In the transition state associated with 1,3-silyl migration, one Si−N bond is broken while one Si−O bond is made at the same time. Hydrogen atoms are not efficient at stabilizing a SiR_3^+ group; thus distances to Si have to remain substantially short in the TS (Si···N = 2.182 Å, Si···O = 2.059 Å for $\mathbf{AmTS2_{qm}}$; Si···N = 2.306 Å, Si···O = 2.114 Å for $\mathbf{AmTS2_{oniom}}$). When the migrating $SiMe_3$ group is entirely treated at the DFT level, the stabilizing electronic inductive effect of the methyl groups is included. In the transition state, the Si···N distance can thus be significantly longer (2.422 Å) without introducing severe destabilization.

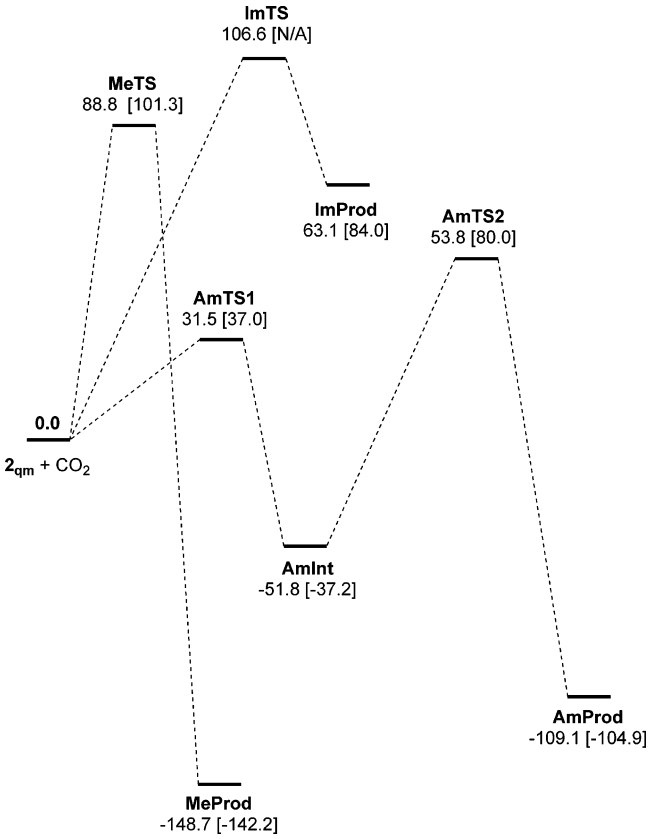

Figure 5. Comparison between the three different pathways computed at the DFT(B3PW91) (energies in kJ·mol^{-1}) and ONIOM(B3PW91:UFF) (values in brackets) levels for the reaction of $\mathbf{2_{qm}}$ ($\mathbf{2_{oniom}}$ in the ONIOM study) with CO_2.

Table 3. Energies (kJ·mol^{-1}, with Respect to Separated Reactants) for the Various Extrema along the Preferred Pathway for CO_2 Reaction with $\mathbf{2}^{+a}$

	AmTS1	AmInt	AmTS2	AmProd
qm	31.5	−51.8	53.8	−109.1
oniom	37.0	−37.2	80.0	−104.9
ONIOM	43.2	−49.0	56.1	−129.5

[a] DFT(B3PW91) results are expressed as qm, while for the ONIOM(B3PW91:UFF) results, oniom corresponds to the situation where the migrating $SiMe_3$ group is modeled by SiH_3 in the QM part and ONIOM to the situation where it is fully considered in the QM part.

Scheme 4. Schematic Representation of the Two Different Insertion Reactions Studied between 2^+ and RNCO: Insertion into the W−N_{amide} Bond with Formation of a W−N Bond (N-AmInt); Insertion into the W−N_{Amide} Bond with Formation of a W−O Bond (O-AmInt)[a]

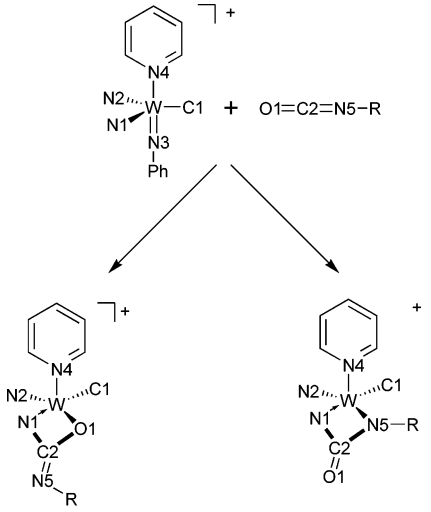

[a] The numbering scheme shown will be used systematically in the theoretical study. For the clarity of the representation, the group N3−Ph has been omitted in the insertion products **N-AmInt** and **O-AmInt**.

Similarly, the Si···O distance is not necessarily short in the TS (2.252 Å). This rather "remote" position of the migrating $SiMe_3$ group in the TS originates from the stabilizing influence of the Me substituents, which is only fully accounted for when $SiMe_3$ is in the QM part. The other consequence of this geometry is a diminution of the steric repulsions. All these aspects explain the value of 56.1 kJ·mol^{-1} (Table 3) obtained for the energy of $\mathbf{AmTS2}_{\mathbf{ONIOM}}$. The electronic influence of $SiMe_3$ vs SiH_3 is clearly illustrated by the energy of the product of migration with an increase by 25 kJ·mol^{-1} in the exothermicity of the overall reaction leading to $\mathbf{Am\text{-}Prod}_{\mathbf{ONIOM}}$ (Table 3).

In conclusion, in the case of the cationic tungsten complex $\mathbf{2}^+$, upon reaction with CO_2, there is one reaction pathway exclusively followed. It consists of the insertion of CO_2 into the W−N_{amide} bond, followed by $SiMe_3$ migration from N to O. The intermediate is not expected to be observed, fully in accord with the experimental observations.

Computed Reaction Mechanism for RNCO. Reaction of $\mathbf{2}^+$ with RNCO follows the same general mechanism as for CO_2: insertion into the W−N_{amide} bond, followed by $SiMe_3$ migration. However, in the case of RNCO, the heterocumulene is not symmetric and the reaction may proceed with two different regiochemistries of insertion (Scheme 4). Experimentally, when R = ^{t}Bu, *p*-tolyl, or phenyl, the insertion proceeds with formation of a W−N bond, whereas a W−O bond is formed when R = 2,6-$C_6H_3{}^i Pr_2$. The insertion reaction to form **N-AmInt** (Scheme 4) therefore seems to be the preferred pathway unless the isocyanate substituent is very bulky. A computational study of the two pathways was carried out at the DFT(B3PW91) level for the model systems $\mathbf{2}_{\mathbf{qm}}$ and MeNCO to determine the main electronic features of the reaction. Then the ONIOM(B3PW91:UFF) method was used to estimate the effect of the bulkiness of the isocyanate R group (R = ^{t}Bu only).

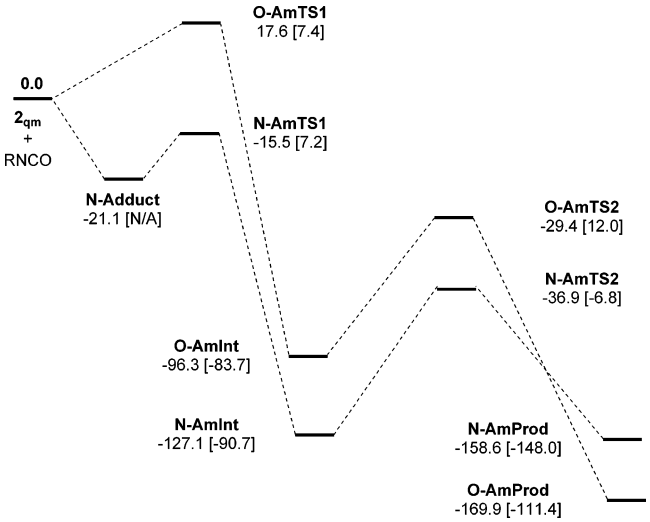

Figure 6. Comparison between the two insertion−$SiMe_3$ migration pathways computed at the DFT(B3PW91) level (energies in kJ·mol^{-1}) and at the ONIOM(B3PW91:UFF) (values in brackets) for the reaction of $\mathbf{2}_{\mathbf{qm}}$ ($\mathbf{2}_{\mathbf{oniom}}$ in the ONIOM study) with RNCO (R = Me in the DFT study and R = ^{t}Bu in the ONIOM study).

Electronic Effects: $\mathbf{2}_{\mathbf{qm}}$ + MeNCO. The two pathways, computed at the B3PW91 level, are shown schematically in Figure 6. The main conclusion is that the path associated with the formation of a W−N bond (**N-AmInt**) is electronically favored over the other one (**O-AmInt**). In particular, the existence of a precomplex (**N-Adduct**) indicates that an initial stabilizing W···N5 interaction orientates the regiochemistry of the insertion (numbering of the atoms is shown in Scheme 4). RNCO are not as poor ligands as CO_2, and the HOMO is higher in energy and heavily weighted on N (although the steric effects of the N substituent should not be neglected). Also, the thermodynamic stability of the insertion products $\mathbf{N\text{-}AmInt}_{\mathbf{qm}}$ ($\Delta_r G$ = −52.8 kJ·mol^{-1}) or $\mathbf{O\text{-}AmInt}_{\mathbf{qm}}$ ($\Delta_r G$ = −21.1 kJ·mol^{-1}) is significantly larger than the corresponding intermediate for CO_2 ($\mathbf{AmInt}_{\mathbf{qm}}$, $\Delta_r G$ = 9.6 kJ·mol^{-1}), thus explaining why they are observed experimentally (real systems $\mathbf{5}^+$, $\mathbf{7}^+$, and $\mathbf{11}^+$) while no intermediate was seen with CO_2.

Views of the extrema located along both pathways are shown in Figures 7 and 8, and selected geometric parameters are given in the SI (Tables S3 and S4). The precomplex $\mathbf{N\text{-}Adduct}_{\mathbf{qm}}$ is not thermodynamically stable ($\Delta_r G$ = 38.6 kJ·mol^{-1}), but it lowers the activation barrier for insertion by creating a stabilizing W···N interaction. In the transition states for insertion $\mathbf{N\text{-}AmTS1}_{\mathbf{qm}}$ and $\mathbf{O\text{-}AmTS1}_{\mathbf{qm}}$, the bond to W (W−N5 = 2.278 Å and W−O1 = 2.208 Å, respectively) is elongated by 10% with respect to that of the corresponding insertion products (W−N5 = 2.071 Å and W−O1 = 2.016 Å, respectively). The corresponding value was 15% for the reaction with CO_2. The developing N1···C2 bond in the TS for insertion ($\mathbf{N\text{-}AmTS1}_{\mathbf{qm}}$ and $\mathbf{O\text{-}AmTS1}_{\mathbf{qm}}$) is 61.5% and 46.5% longer than in the corresponding products ($\mathbf{N\text{-}AmInt}_{\mathbf{qm}}$ and $\mathbf{O\text{-}AmInt}_{\mathbf{qm}}$), respectively. The corresponding value for

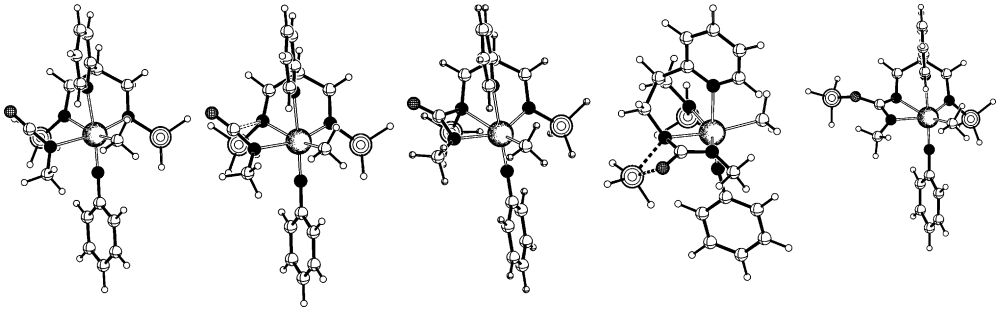

Figure 7. Optimized geometry (B3PW91) for the extrema along the pathway for insertion of MeNCO into the W−N$_{amide}$ bond of **2$_{qm}$** with formation of a W−N bond. Energy values (Gibbs free energy values in parentheses) are given relative to separated reactants **2$_{qm}$** and MeNCO in kJ·mol^{-1}.

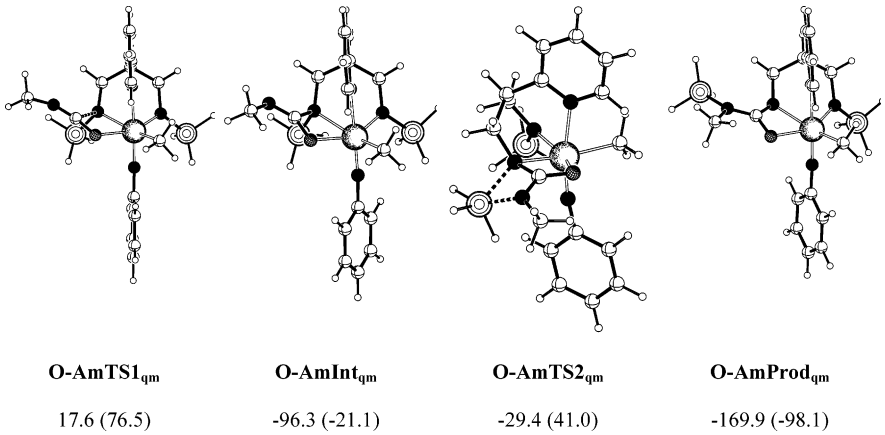

Figure 8. Optimized geometry (B3PW91) for the extrema along the pathway for insertion of MeNCO into the W−N$_{amide}$ bond of **2$_{qm}$** with formation of a W−O bond. Energy values (Gibbs free energy values in parentheses) are given relative to separated reactants **2$_{qm}$** and MeNCO in kJ·mol^{-1}.

insertion of CO_2 is 50%. This indicates that **N-AmTS1$_{qm}$** is an earlier TS than **O-AmTS1$_{qm}$** and is thus associated with a lower activation barrier (49.4 vs 76.5 kJ·mol^{-1}), as both reactions are exothermic. Interestingly, the activation barrier corresponding to **O-AmTS1$_{qm}$** is very similar to that for **AmTS1$_{qm}$** in the CO_2 insertion (76.5 vs 81.5 kJ·mol^{-1}). In both cases the N1···C2 bond is longer than the value in the product by 50%, but the W···O distance is 10% and 15% longer, respectively. This seems to indicate that W···O interaction in the TS is not a determining factor because O is not a good enough donor. Thus the regiochemistry of the insertion is essentially driven by the initially stabilizing W···N interaction resulting from donation from the MeNCO HOMO to W. However, the activation barrier corresponds to the bond-forming process between N1 and C2.

The second step of the insertion is $SiMe_3$ migration from N1 to either O1 (**N-AmTS2$_{qm}$**) or N5 (**O-AmTS2$_{qm}$**), very similar to the reaction in the case of CO_2. The migration from N1 to N5 (**O-AmTS2$_{qm}$**) is easier than that from N1 to O1 (**N-AmTS2$_{qm}$**) with an activation barrier $\Delta_r G^{\#}$ (estimated from the intermediate) of 62.2 and 89.4 kJ·mol^{-1}, respectively. The corresponding $\Delta_r E^{\#}$ values (Figure 6) are very close to the $\Delta_r G^{\#}$ values (66.9 and 90.2 kJ·mol^{-1}, respectively). Experimentally, the activation barrier for N1 to N5 1,3-$SiMe_3$ migration associated with the formation of **12**$^+$ from **11**$^+$ was evaluated to be $\Delta_r G^{\#} = 93.8 \pm 5$ kJ·mol^{-1} at 298 K. Thus the calculated value of 62.2 kJ·mol^{-1} is only in qualitative agreement with the experimental results. However, the experimental system corresponds to a bulky group (2,6-$C_6H_3{}^iPr_2$), whereas the calculated system was MeNCO reacting with **2$_{qm}$**, in which the actual steric bulk of both the isocyanate and the $SiMe_3$ group is missing. It is therefore important to take into account the sterics of the system (and probably also solvent reorganization effects for these ionic compounds). The DFT study has, however, shown that there is indeed an electronic origin in the regiochemistry of the insertion and that both the insertion intermediate and 1,3-migrated products are more stable than the reactants, accounting for their experimental observation.

Steric Effects: 2$_{oniom}$ + ^{t}BuNCO. The two reaction pathways were computed at the ONIOM(B3PW91:UFF) level, and only ^{t}BuNCO was considered as a substrate. In this ONIOM study, the QM parts were the same as those in the DFT cases, and the "missing" Me groups were added and treated at the MM level (UFF). The ONIOM energy values are given in brackets in Figure 6. Some geometric parameters are given in the SI (Tables S3 and S4).

The first important difference with respect to the DFT study is the absence of a precomplex similar to **N−Adduct$_{qm}$**. In fact the W···N5 distance in **N-Adduct$_{qm}$** (2.411 Å) has the same value in the TS optimized at the ONIOM level, **N-AmTS1$_{oniom}$**. This TS for insertion brings the ^{t}Bu group close to the methyl ligand, and

Table 4. DFT(B3PW91) Gibbs Free Energies (kJ·mol^{-1}, with Respect to Separated Reactants) for the Various Extrema along the Three Pathways Studied for the Reaction of CO_2 with M(NPh)(N_2N_{qm})(Me) (M = W^+, Ta)

	AmTS1	AmInt	AmTS2	AmProd	MeTS	MeProd	ImTS	ImProd
W^+	81.5	9.6	111.8	−52.6	137.9	−94.8	157.4	123.7
Ta	61.0	−19.5	77.2	−50.5	92.5	−131.3	83.5	10.4

steric repulsions develop, preventing the formation of a stable adduct. The electronic preference for the regiochemistry of the insertion is destroyed by the steric repulsions, and the two transition states are now isoenergetic (7.2 kJ·mol^{-1} for **N-AmTS1$_{oniom}$**; 7.4 kJ·mol^{-1} for **O-AmTS1$_{oniom}$**). These results qualitatively show that the regiochemistry of the insertion depends on the bulk of the isocyanate substituent, even though the electronic preference is to make a W−N bond in the insertion product. However, a quantitative prediction of which pathway is followed for a given R group is difficult because the two possible cases are associated with activation barriers of similar energy values. Nevertheless, the fact that with a bulky ^{t}Bu group both TSs are of similar energy tends to indicate that the size of the substituent is not a critical parameter and that its size has to be considerable to alter the regiochemistry. Hence with isocyanate N-substituents *tert*-butyl and *p*-tolyl the RNCO insertion leading to **N-AmInt** is observed (**5**$^+$ and **7**$^+$ experimentally), whereas only with a very bulky group (R = 2,6-$C_6H_3{}^iPr_2$) is the other isomer obtained (**11**$^+$).

The size of the substituent also plays an important role in the $SiMe_3$ migration step. As expected the inclusion of the Me groups on Si and in R = ^{t}Bu increases the activation barrier for $SiMe_3$ migration from N1 to N5 in **O-AmInt**, as both bulky groups are brought in close contact in the TS. There is a 30 kJ·mol^{-1} increase in the value of $\Delta_r E^{\#}$ (energy difference between **O-AmTS2$_{oniom}$** and **O-AmInt$_{oniom}$**) with a value computed to be 95.7 kJ·mol^{-1} at the ONIOM level (66.9 kJ·mol^{-1} at the DFT level, Figure 6). For the other regioisomer, **N-AmInt**, the activation barrier is slightly lower at the ONIOM level but still of comparable value with respect to the DFT case (83.9 kJ·mol^{-1} with ONIOM, 90.2 kJ·mol^{-1} with DFT), showing that the bulk of the R group has little influence on the $SiMe_3$ migration within **N-AmInt**.

In conclusion of the ONIOM study, the precise bulk of the isocyanate R group has an important influence on the regiochemistry of the insertion reaction. However, the electronic preference for making a W···N interaction is strong and the R group has to be very bulky to prevent such an approach. The isocyanate-originated R group also has an influence on the 1,3-$SiMe_3$ migration in the case where the alternate regioisomer **O-AmInt** has been obtained. The repulsion between migrating $SiMe_3$ and the isocyanate R group increases the activation barrier, leading to a longer lived intermediate, as observed experimentally.

Role of the Metal: DFT Calculations with Ta. Experimentally, the reactions of CO_2 with the group 5 *tert*-butyl imido compounds M(N^tBu)(N_2N_{py})Cl(py) (M = Nb (**13**) or Ta (**14**)) or Ta(N^tBu)(N_2N_{py})(Me) are not as well-controlled as with [W(NPh)(N_2N_{py})(Me)]$^+$, and mixtures of products are obtained. For the Cl systems **13** and **14**, observation of ^{t}BuNCO as a side product suggests that cycloaddition to Ta=N^tBu is a competitive pathway. We have therefore carried out a DFT(B3PW91) study of the reaction of CO_2 with the strictly isoelectronic phenylimido compound Ta(NPh)(N_2N_{qm})(Me), where only the nature of the metal center has been changed.

Table 5. Selected NBO Results Obtained on the DFT(B3PW91) Optimized Geometries for M(NPh)(N_2N_{py})(Me) (M = W^+, Ta)[a]

	π(M−N1)		π_1(M−N3)		π_2(M−N3)	
	%N	ϵ	%N	ϵ	%N	ϵ
W^+	89.2	−0.091	73.3	−0.297	88.6	−0.287
Ta	92.7	−0.145	78.0	−0.194	81.7	−0.166

[a] The π-bonds correspond to the results of the NBO search for the best Lewis structure. %N gives in each π-bond the contribution of the hybrid localized on N (100% p character) to the bond orbital and ϵ gives the energy (au) as estimated by the NBO procedure. N1 corresponds to the amido group involved in the insertion reaction, and N3 corresponds to the imido group.

In Table 4, the Gibbs free energy values of the various extrema located on the potential energy surface are given. With Ta, the amide insertion/1,3-$SiMe_3$ migration pathway is still the kinetically preferred one, and it is associated with lower activation barriers than with W^+. However, the activation barrier to cycloaddition at M=N_{imide} drops from a value of 157.4 kJ·mol^{-1} (W^+) to a competitive value of 83.5 kJ·mol^{-1} (Ta). Therefore, for Ta, the situation is strikingly different and no single pathway is very strongly preferred. This explains the observation of a mixture of products. Also, the fact that the cycloaddition is possible is in agreement with the experimental observation of ^{t}BuNCO. In the case of Ta the intermediate **AmInt** is thermodynamically more stable that the separated reactants, thus adding one possible component to the reaction mixture.

The difference in behavior between the W^+ and Ta complexes finds its origin in the energies of the orbitals that play an important role in the reaction with CO_2. A comparative natural bonding orbital (NBO)[44] study of the complexes [W(NPh)(N_2N_{qm})(Me)]$^+$ and Ta(NPh)(N_2N_{qm})(Me) yielded the results reported in Table 5. Due to the cationic nature of the W complex, the bond distances from N to the metal center are shorter (W−N1 = 1.928 Å, W−N3 = 1.747 Å; Ta−N1 = 2.015 Å, Ta−N3 = 1.802 Å; the numbering scheme is shown in Scheme 3). The two π-bonds of the imido linkage are at a significantly lower energy for the W system (Table 5) and are thus less available for reaction with CO_2, consistent with experimental observations for **2**$^+$. The M−N_{amide} π-bond (essentially a N lone pair, see Table 5) is constructed with a metal d AO also used in the M−C bond (see below).

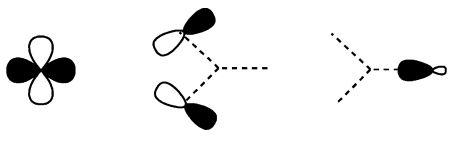

Consequently, depending on the effective electronegativity of the metal, the combinations of these three

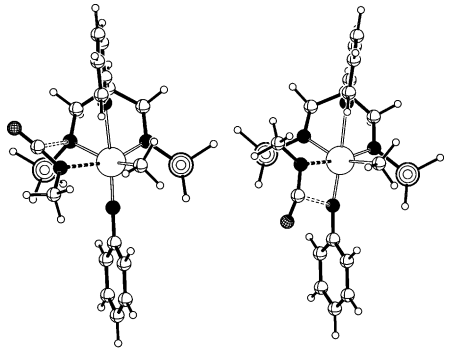

Figure 9. Optimized geometry (B3PW91) for the transition states associated with the insertion of MeNCO into the Ta−N_{amide} bond (**TaN-AmTS1**) or with the cycloaddition to the Ta−N_{imide} bond (**TaN-ImTS**) of Ta(N_2N_{qm})(NPh)(Me). Energy values (Gibbs free energy values in parentheses) are given relative to separated reactants Ta(N_2N_{qm})(NPh)(Me) and MeNCO in kJ·mol^{-1}.

AOs may yield different results. In the case of W the lone pair centered on N1 is at a higher energy than in the case of Ta. Overall the more efficient π-donation in **2_{qm}** results in deeper π-bonds for the imido linkage and higher lone pair energy for the amido group in the case of W^+ with respect to Ta. This situation selects one pathway among the possible ones in the case of W^+. For Ta, the discrimination is less efficient, as the imido π-bonds and the amido lone pairs are of comparable energy.

Interestingly, the reaction of **13** or **14** with ^{t}BuNCO is selective, and only insertion into the M−N_{amide} bond followed by 1,3 $SiMe_3$ migration is observed. We therefore studied computationally some aspects of the reaction of Ta(N_2N_{qm})(NPh)(Me) with MeNCO. Only DFT calculations have been performed, and the TS for insertion into the Ta−N_{amide} bond, **TaN-AmTS1**, and the TS for cycloaddition, **TaN-ImTS**, have been located (Figure 9). With respect to separated reactants, the Gibbs free energies of both TS are lower than for the reaction with CO_2 (see Table 4). This is due to the stabilizing interaction between the isocyanate nitrogen atom and the metal center in both systems. The electronic energy of **TaN-AmTS1** is even lower than that of the separated reactants, clearly showing the electronic stabilization.

However, the energy difference between the two TS structures is of the same magnitude as for the CO_2 analogue (Table 4). Therefore the selectivity in reactions with RNCO is not related to a particular electronic effect associated with a given site of reaction, and thus is not accounted for by the DFT calculations. Nevertheless, reactions with RNCO are more sensitive to the actual bulk of the system. In the transition states **AmTS1** and **ImTS** associated with reactions with CO_2, the Ta···O bond distances are 2.514 and 2.315 Å, respectively. For the reactions with MeNCO, the Ta···N bond distance in the corresponding TS, **TaN-AmTS1** and **TaN-ImTS**, are 2.363 and 2.238 Å, respectively. We may therefore expect that for ^{t}BuNCO strong steric repulsions are likely to develop in the TS for cycloaddition, rendering this pathway energetically prohibitive. As a matter of fact, our attempts to optimize a TS analogous to **TaN-AmTS1** at the ONIOM level failed, as the ^{t}BuNCO dissociated during the optimization procedure.

Conclusions

The complexes [W(NPh)(N_2N_{py})Me]$^+$ (**2^+**), Ta(N^tBu)(N_2N_{py})Me, M(N^tBu)(N_2N_{py})Cl(py) (M = Nb (**13**) or Ta (**14**)), and Ti(N^tBu)(N_2N_{py})(py) (**19**) have several potential sites of reactivity with heterocumulenes. In all cases with isocyanates, and for **2^+** with CO_2, the reactions exclusively proceed via insertion in M−N_{amide} bonds followed by 1,3-$SiMe_3$ migrations. For **2^+** the intermediates can be observed only in the reactions with isocyanates due to stronger W−N vs W−O bonding. Despite thermodynamic preferences in the tungsten systems, the reactions are governed by frontier orbital control and kinetic considerations. Steric preferences (with regard to the orientation of isocyanate substrate insertion) play a secondary role in the reaction outcomes. In the isoelectronic group 5 model system Ta(NPh)(N_2N_{py})Me there is a less pronounced stability of the imido bond, which leads to less well-defined reaction pathways with CO_2 since attack at M−N_{amide} and M=N_{imide} is kinetically more equally favored. The better defined reactions of **13** and **14** with RNCO may be attributed to steric hindrance disfavoring attack at M=N^{t}Bu in these cases, and this is probably also the case for the titanium system **19**.

Experimental Section

General Methods and Instrumentation. All manipulations were carried out using standard Schlenk line or drybox techniques under an atmosphere of argon or dinitrogen. Solvents were predried over activated 4 Å molecular sieves and were refluxed over potassium (benzene), sodium/potassium alloy (pentane), or calcium hydride (dichloromethane) under a dinitrogen atmosphere and collected by distillation. Deuterated solvents were dried over potassium (C_6D_6) or phosphorus pentoxide (CD_2Cl_2), distilled under reduced pressure, and stored under dinitrogen in Teflon valve ampules. NMR samples were prepared under dinitrogen or Ar in 5 mm J. Young NMR tubes.

^{1}H, ^{13}C{^{1}H}, ^{13}C, ^{19}F, and ^{11}B{^{1}H} NMR spectra were recorded on Varian Mercury-VX 300 and Varian Unity Plus 500 spectrometers. ^{1}H and ^{13}C assignments were confirmed when necessary with the use of DEPT-135, DEPT-90, and two-dimensional ^{1}H−^{1}H and ^{13}C−^{1}H NMR experiments. ^{1}H and ^{13}C spectra were referenced internally to residual protio-solvent (^{1}H) or solvent (^{13}C) resonances and are reported relative to tetramethylsilane (δ = 0 ppm). ^{19}F and ^{11}B spectra were referenced externally to $CFCl_3$ (^{19}F) and BF_3·Et_2O (^{11}B). Chemical shifts are quoted in δ (ppm) and coupling constants in hertz.

Infrared spectra were prepared as KBr pellets or Nujol mulls between KBr or NaCl plates and were recorded on Perkin-Elmer 1600 and 1710 series FTIR spectrometers. Infrared data are quoted in wavenumbers (cm^{-1}). Mass spectra were recorded by the mass spectrometry service of the University of Oxford Chemistry Department, and elemental analyses by the analytical services of the University of Oxford Inorganic Chemistry Laboratory.

Literature Preparations. The compounds Nb(N^tBu)(N_2N_{py})Cl(py) (**13**), Ta(N^tBu)(N_2N_{py})Cl(py) (**14**),[25] Ta(N^tBu)(N_2N_{py})Me,[27] W(NPh)(N_2N_{py})Me_2 (**1**),[26] and [W(NPh)(N_2N_{py})-

(44) Reed, A. E.; Curtiss, L. A.; Weinhold, F. *Chem. Rev.* **1988**, *88*, 899.

Me][$MeBAr^F_3$] (**2-MeBAr$^F_3$**),[27] and their corresponding ^{13}C- and d-isotopomers, were prepared according to published methods. The compound BAr^F_3 was provided by DSM Research. Liquid isocyanates and CS_2 were degassed by three freeze−pump−thaw cycles. All other compounds and reagents were purchased from commercial suppliers and used without further purification.

[W(NPh)(MeC(2-C_5H_4N)(CH_2NSiMe_3)($CH_2NC(OSiMe_3)$-O)Me][MeBAr$^F_3$] (3-MeBAr$^F_3$). To a stirred solution of [W(NPh)(N_2N_{py})Me_2] (**1**) (150 mg, 0.24 mmol) in CH_2Cl_2 (20 mL) cooled to 0 °C was added a solution of BAr^F_3 (125 mg, 0.24 mmol) in CH_2Cl_2 (20 mL). The solution was degassed by three freeze−pump−thaw cycles before adding CO_2 (1 atm). After stirring at room temperature for 1 h the solvent was removed under reduced pressure to afford **3-MeBAr$^F_3$** as a golden-brown solid. Yield: 96 mg (34%). ^1H NMR (CD_2Cl_2, 500.0 MHz, 293 K): 8.80 (1 H, dd, H^6, $^3J(H^5H^6)$ = 5.9 Hz, $^4J(H^4H^6)$ = 1.5 Hz), 8.21 (1 H, td, H^4, $^3J(H^3H^4H^5)$ = 7.8 Hz, $^4J(H^4H^6)$ = 1.7 Hz), 7.83 (1 H, d, H^3, $^3J(H^3H^4)$ = 8.3 Hz), 7.66 (1 H, td, H^5, $^3J(H^4H^5H^6)$ = 5.6 Hz, $^4J(H^3H^5)$ = 1.3 Hz), 7.57 (2 H, t, *m*-C_6H_5, ^3J = 7.6 Hz), 7.33 (2 H, d, *o*-C_6H_5, ^3J = 7.6 Hz), 7.26 (1 H, t, *p*-C_6H_5, ^3J = 7.6 Hz), 4.31 (1 H, d, C*H*HNSiMe$_3$, ^2J = 16.1 Hz), 4.10 (1 H, d, CH*H*NSiMe$_3$, ^2J = 16.4 Hz), 3.80 (1 H, d, C*H*HNCOSiMe$_3$, ^2J = 12.4 Hz), 3.08 (1 H, d, CH*H*NCOSiMe$_3$, ^2J = 12.7 Hz), 1.68 (3 H, s, *Me*CCH_2), 1.40 (3 H, s, WMe, ^2J(WH) = 6.8 Hz (15%)), 0.45 (3 H, br s, BMe), 0.40 (9 H, s, NSiMe$_3$), 0.04 (9 H, s, OSiMe$_3$) ppm. ^{13}C NMR (CD_2Cl_2, 125.7 MHz, 293 K): 166.6 (CO), 162.6 (C^2), 155.0 (*ipso*-C_6H_5), 151.2 (C,[6] ^1J(CH) = 166 Hz), 148.7 (C_6F_5, ^1J(CF) = 239 Hz), 144.1 (*o*-C_6H_5, ^1J(CH) = 160 Hz), 137.8 (C_6F_5, ^1J(CF) = 251 Hz), 136.7 (C_6F_5, ^1J(CF) = 251 Hz), 130.9 (C,[4] ^1J(CH) = 166 Hz), 130.2 (*m*-C_6H_5, ^1J(CH) = 157 Hz), 128.7 (*p*-C_6H_5, ^1J(CH) = 166 Hz), 126.4 (C,[5] ^1J(CH) = 164 Hz), 123.4 (C^3, ^1J(CH) = 167 Hz), 66.0 (2 × Me*C*CH_2, ^1J(CH) = 131 Hz), 51.3 (*C*(CH_2NSiMe_3)), 44.5 (WMe, ^1J(CH) = 125.0 Hz, ^1J(WC) = 92 Hz (15%)), 20.4 (*Me*CCH_2, ^1J(CH) = 129 Hz), 10.5 (BMe, ^1J(CH) = 117.4 Hz), 0.8 (NSiMe$_3$, ^1J(CH) = 122 Hz), −1.2 (OSiMe$_3$, ^1J(CH) = 120 Hz) ppm. ^{19}F NMR (CD_2Cl_2, 282.2 MHz, 293 K): −133.4 (6 F, d, *o*-Ar^F, ^3J = 19.8 Hz), −165.6 (6 F, app. t, *p*-Ar^F, app. ^3J = 19.8 Hz), −168.1 (3 F, t, *m*-Ar^F, ^3J = 22.7 Hz) ppm. $^{11}B\{^1H\}$ NMR (CD_2Cl_2, 160.4 MHz, 293 K): −14.7 (br s, $MeBAr^F_3$) ppm. IR (KBr pellet): 3066 (w), 2958 (m), 2908 (m), 2852 (w), 1640 (m), 1608 (m), 1552 (s), 1510 (s), 1482 (s), 1450 (s), 1384 (m), 1356 (m), 1258 (s), 1230 (w), 1170 (w), 1146 (w), 1086 (s), 1032 (m), 1020 (m), 966 (s), 952 (s), 934 (m), 838 (s), 816 (m), 786 (m), 762 (m), 732 (w), 688 (m), 660 (w), 646 (w), 594 (w), 582 (w), 570 (w), 542 (w), 512 (w), 420 (w), 408 (w) cm^{-1}. Anal. Calcd for $C_{42}H_{40}BF_{15}N_4O_2Si_2W$: C, 43.2; H, 3.5; N, 4.8. Found: C, 43.0; H, 3.8; N, 4.9.

[W(NPh)(MeC(2-C_5H_4N)(CH_2NSiMe_3)($CH_2NC(SSiMe_3)S$)-Me][MeBAr$^F_3$] (4-MeBAr$^F_3$). To a stirred solution of [W(NPh)(N_2N_{py})Me_2] (**1**) (150 mg, 0.24 mmol) in CH_2Cl_2 (20 mL) cooled to 0 °C was added a solution of BAr^F_3 (125 mg, 0.24 mmol) in CH_2Cl_2 (20 mL). To the stirred reaction was added CS_2 (19 mg, 14.6 μL, 0.24 mmol). After stirring at room temperature for 18 h the solvent was removed under reduced pressure to afford **4-MeBAr$^F_3$** as a golden-brown solid. Yield: 192 mg (66%). ^1H NMR (CD_2Cl_2, 500.0 MHz, 293 K): 8.99 (1 H, dd, H^6, $^3J(H^5H^6)$ = 5.9 Hz, $^4J(H^4H^6)$ = 1.5 Hz), 8.20 (1 H, td, H^4, $^3J(H^3H^4H^5)$ = 7.8 Hz, $^4J(H^4H^6)$ = 1.5 Hz), 7.84 (1 H, d, H^3, $^3J(H^3H^4)$ = 7.8 Hz), 7.65−7.58 (3 H, m, H^5, *m*-C_6H_5), 7.38 (2 H, dd, *o*-C_6H_5, ^3J = 8.8 Hz, ^4J = 1.5 Hz), 7.30 (1 H, t, *p*-C_6H_5, ^3J = 7.3 Hz), 4.30 (1 H, d, C*H*HNCOSiMe$_3$, ^2J = 12.2 Hz), 4.23 (1 H, d, C*H*HNSiMe$_3$, ^2J = 16.1 Hz), 4.08 (1 H, d, CH*H*NSiMe$_3$, ^2J = 16.1 Hz), 3.36 (1 H, d, CH*H*NCOSiMe$_3$, ^2J = 12.2 Hz), 1.75 (3 H, s, *Me*CCH_2), 1.30 (3 H, s, WMe, ^2J(WH) = 7.8 Hz (15%)), 0.43 (3 H, br s, BMe), 0.41 (9 H, s, NSiMe$_3$), 0.28 (9 H, s, OSiMe$_3$) ppm. ^{13}C NMR (CD_2Cl_2, 125.7 MHz, 293 K): 160.3 (C^2), 153.4 (*ipso*-C_6H_5), 150.9 (C^6, ^1J(CH) = 168 Hz), 148.7 (C_6F_5, ^1J(CF) = 239 Hz), 142.3 (C^4, ^1J(CH) = 163 Hz), 137.8 (C_6F_5, ^1J(CF) = 251 Hz), 136.7 (C_6F_5, ^1J(CF) = 251 Hz), 130.2 (CS), 129.0 (*o*-C_6H_5, ^1J(CH) = 157 Hz), 128.9 (*m*-C_6H_5, ^1J(CH) = 154 Hz), 128.2 (*p*-C_6H_5, ^1J(CH) = 159 Hz), 124.7 (C,[5] ^1J(CH) = 160 Hz), 122.4 (C^3, ^1J(CH) = 166 Hz), 65.6 (*C*H_2NSiMe_3, ^1J(CH) = 137 Hz), 58.5 (*C*(CH_2NSiMe_3)$_2$), 53.7 (*C*$H_2NCOSiMe_3$, ^1J(CH) = 138 Hz), 47.4 (WMe, ^1J(CH) = 124 Hz), 21.6 (*Me*CCH_2, ^1J(CH) = 128 Hz), 10.5 (BMe), 1.9 (NSiMe$_3$, ^1J(CH) = 121 Hz), 1.3 (OSiMe$_3$, ^1J(CH) = 124 Hz) ppm. ^{19}F NMR (CD_2Cl_2, 282.2 MHz, 293 K): −133.4 (6 F, d, *o*-Ar^F, ^3J = 19.8 Hz), −165.6 (6 F, app. t, *p*-Ar^F, app. ^3J = 19.8 Hz), −168.1 (3 F, t, *m*-Ar^F, ^3J = 22.7 Hz) ppm. $^{11}B\{^1H\}$ NMR (CD_2Cl_2, 160.4 MHz, 293 K): −14.7 (br s, $MeBAr^F_3$) ppm. IR (KBr pellet): 3064 (w), 2958 (s), 2904 (m), 2848 (w), 1640 (s), 1608 (s), 1510 (s), 1448 (s), 1384 (m), 1356 (m), 1258 (s), 1180 (w), 1170 (w), 1086 (s), 1048 (m), 1020 (m), 968 (s), 952 (s), 934 (s), 838 (s), 806 (s), 784 (m), 734 (w), 686 (m), 660 (w), 646 (w), 628 (w), 604 (w), 570 (w), 556 (w), 512 (w), 438 (w), 406 (w) cm^{-1}. Anal. Calcd for $C_{42}H_{40}BF_{15}N_4S_2Si_2W$: C, 42.0; H, 3.4; N, 4.7. Found: C, 42.6; H, 3.4; N, 5.0.

[W(NPh){MeC(2-C_5H_4N)(CH_2NSiMe_3)($CH_2N(SiMe_3)C$-(O)N^{t}Bu}Me][MeBAr$^F_3$] (5-MeBAr$^F_3$). To a stirred solution of [W(NPh)(N_2N_{py})Me_2] (**1**) (200 mg, 0.324 mmol) in CH_2Cl_2 was added a solution of BAr^F_3 (166 mg, 0.324 mmol) in CH_2Cl_2 (10 mL). The resulting brown solution was stirred for 1 min before cooling to −78 °C. The reaction temperature was maintained at −78 °C for the addition of ^{t}BuNCO (37 μL, 32.1 mg, 0.324 mmol) and the subsequent workup. The reaction was stirred for 1 h before concentrating to ca. 10 mL under reduced pressure. Cold (−78 °C) pentane (30 mL) was added, which caused a brown oil to separate from the solution. The supernatant was decanted, and the oil was washed with pentane (3 × 5 mL) and dried in vacuo to yield [W(NPh){MeC-(2-C_5H_4N)(CH_2NSiMe_3)($CH_2N(SiMe_3)C(O)N^tBu$}Me][Me-BAr^F_3] as a brown solid. Yield: 202 mg (51%). ^1H NMR (CD_2Cl_2, 500.0 MHz, 193 K): 8.72 (1 H, d, H^6, $^3J(H^5H^6)$ = 5.4 Hz), 8.14 (1 H, t, H^4, $^3J(H^3H^4H^5)$ = 7.8 Hz), 7.74 (1 H, d, H^3, $^3J(H^3H^4)$ = 8.3 Hz), 7.60 (1 H, t, H^5, $^3J(H^4H^5H^6)$ = 6.8 Hz), 7.56 (2 H, t, *m*-C_6H_5, ^3J = 7.8 Hz), 7.26 (2 H, d, *o*-C_6H_5, ^3J = 7.8 Hz), 7.24 (1 H, t, *p*-C_6H_5, ^3J = 7.8 Hz), 4.11 (1 H, d, C*H*HNSiMe$_3$ "out", ^2J = 17.1 Hz), 3.90 (1 H, d, CH*H*NSiMe$_3$ "in", ^2J = 17.1 Hz), 3.81 (1 H, d, CH*H*NCN^{t}Bu "out", ^2J = 14.2 Hz), 2.65 (1 H, d, C*H*HNCN^{t}Bu "in", ^2J = 14.2 Hz), 1.65 (3 H, s, *Me*CCH_2), 1.46 (3 H, s, WMe), 1.15 (9 H, s, CMe_3), 0.30 (12 H, br s, NC(O)NSi*Me*$_3$, BMe), 0.14 (18 H, s, CH_2NSiMe_3) ppm. $^{13}C\{^1H\}$ NMR (CD_2Cl_2, 125.7 MHz, 193 K): 157.9 (C^2), 157.5 (C═O), 152.6 (*ipso*-C_6H_5), 149.9 (C^6), 147.2 (C_6F_5, ^1J(CF) = 239 Hz), 141.7 (C^4), 136.6 (C_6F_5, ^1J(CF) = 251 Hz), 135.8 (C_6F_5, ^1J(CF) = 251 Hz), 128.5 (*m*-C_6H_5), 128.1 (*p*-C_6H_5), 125.3 (*o*-C_6H_5), 124.3 (C^5), 121.0 (C^3), 63.6 (*C*$H_2N(SiMe_3)CO$), 60.9 (*C*(CH_2NSiMe_3)$_2$), 57.6 (*C*Me_3), 50.4 (*C*H_2NSiMe_3), 41.2 (WMe, ^1J(CH) = 130 Hz, ^1J(WC) = 106 Hz (15%)), 29.3 (C*Me*$_3$), 22.2 (*Me*CCH_2), 9.1 (BMe), 0.9 ($SiMe_3$) ppm. ^{19}F NMR (CD_2Cl_2, 282.2 MHz, 193 K): −135.5 (6 F, d, *o*-Ar^F, ^3J = 19.8 Hz), −166.8 (6 F, app. t, *p*-Ar^F, app. ^3J = 19.8 Hz), −169.7 (3 F, t, *m*-Ar^F, ^3J = 22.7 Hz) ppm. $^{11}B\{^1H\}$ NMR (CD_2Cl_2, 160.4 MHz, 193 K): −15.0 (br s, $MeBAr^F_3$) ppm. IR (KBr pellet): 2964 (m), 2906 (w), 2856 (w), 1642 (m), 1608 (m), 1590 (m), 1510 (s), 1460 (s), 1384 (m), 1364 (m), 1260 (s), 1020 (w), 966 (m), 952 (m), 934 (m), 844 (s), 800 (m), 762 (m), 688 (w), 660 (w), 644 (w), 620 (w), 598 (w), 566 (w), 436 (w) cm^{-1}. Anal. Calcd for $C_{46}H_{49}BF_{15}N_5OSi_2W$: C, 45.2; H, 4.2; N, 5.7. Found: C, 45.1; H, 4.1; N, 5.7.

[W(NPh)(MeC(2-C_5H_4N)(CH_2NSiMe_3)($CH_2NC(OSiMe_3)$-N^{t}Bu)Me][MeBAr$^F_3$] (6-MeBAr$^F_3$). To a stirred solution of [W(NPh)(N_2N_{py})Me_2] (**1**) (150 mg, 0.24 mmol) in CH_2Cl_2 (20 mL) cooled to 0 °C was added a solution of BAr^F_3 (125 mg, 0.24 mmol) in CH_2Cl_2 (20 mL). To the stirred reaction was added ^{t}BuNCO (24 mg, 28 μL, 0.24 mmol). After stirring at room temperature for 1 h the solvent was removed under reduced pressure to afford **6-MeBAr$^F_3$** as a golden-brown solid. Yield: 155 mg (52%). ^1H NMR (CD_2Cl_2, 500.0 MHz, 293 K): 8.79 (1 H, dd, H^6, $^3J(H^5H^6)$ = 7.8 Hz, $^4J(H^4H^6)$ = 1.2 Hz), 8.15

(1 H, td, H^4, $^3J(H^3H^4H^5) = 7.5$ Hz, $^4J(H^4H^6) = 1.7$ Hz), 7.78 (1 H, d, H^3, $^3J(H^3H^4) = 7.7$ Hz), 7.60−7.53 (3 H, overlapping m, H^5, *m*-C_6H_5), 7.30 (2 H, dd, *o*-C_6H_5, $^3J = 8.7$ Hz, $^4J = 1.2$ Hz), 7.24 (1 H, t, *p*-C_6H_5, $^3J = 7.5$ Hz), 4.13 (1 H, d, C*H*HNSiMe$_3$, $^2J = 16.1$ Hz), 3.95 (1 H, d, CH*H*NSiMe$_3$, $^2J = 16.3$ Hz), 3.38 (1 H, d, C*H*HNCOSiMe$_3$, $^2J = 11.7$ Hz), 3.05 (1 H, d, CH*H*NCOSiMe$_3$, $^2J = 11.7$ Hz), 1.66 (3 H, s, *Me*CCH$_2$), 1.20 (3 H, s, WMe, ^2J(WH) = 6.3 Hz (15%)), 1.08 (9 H, s, C*Me*$_3$), 0.45 (3 H, br s, BMe), 0.33 (9 H, s, NSiMe$_3$), 0.27 (9 H, s, OSiMe$_3$) ppm. ^{13}C NMR (CD_2Cl_2, 125.7 MHz, 293 K): 161.6 (*C*N^{t}Bu), 160.6 (C^2), 154.1 (*ipso*-C_6H_5), 148.7 (C_6F_5, ^1J(CF) = 239 Hz), 142.1 (C^6, ^1J(CH) = 166 Hz), 137.8 (C_6F_5, ^1J(CF) = 251 Hz), 136.7 (C_6F_5, ^1J(CF) = 251 Hz), 128.9 (*o*-C_6H_5, ^1J(CH) = 159 Hz), 128.8 (*m*-C_6H_5, ^1J(CH) = 158 Hz), 127.6 (*p*-C_6H_5, ^1J(CH) = 156 Hz), 127.5 (C,[4] ^1J(CH) = 165 Hz), 124.5 (C,[5] ^1J(CH) = 163 Hz), 121.6 (C^3, ^1J(CH) = 167 Hz), 64.4 (*C*H$_2$-NSiMe$_3$, ^1J(CH) = 135 Hz), 55.6 (*C*Me$_3$), 54.5 (*C*(CH$_2$NSiMe$_3$)$_2$), 51.7 (*C*H$_2$NCOSiMe$_3$, ^1J(CH) = 139 Hz), 42.1 (WMe, ^1J(CH) = 123 Hz, ^1J(WC) = 97 Hz (15%)), 31.4 (C*Me*$_3$, ^1J(CH) = 126 Hz), 21.7 (*Me*CCH$_2$, ^1J(CH) = 128 Hz), 1.9 (NSiMe$_3$, ^1J(CH) = 121 Hz), 0.6 (OSiMe$_3$, ^1J(CH) = 122 Hz) ppm. ^{19}F NMR (CD_2Cl_2, 282.2 MHz, 293 K): −133.4 (6 F, d, *o*-Ar^F, $^3J = 19.8$ Hz), −165.6 (6 F, app. t, *p*-Ar^F, app. $^3J = 19.8$ Hz), −168.1 (3 F, t, *m*-Ar^F, $^3J = 22.7$ Hz) ppm. ^{11}B{^{1}H} NMR (CD_2Cl_2, 160.4 MHz, 293 K): −14.7 (br s, MeBAr$^F_3$) ppm. IR (KBr pellet): 3066 (w), 2972 (s), 2906 (s), 2854 (m), 2258 (w), 1640 (m), 1608 (m), 1584 (w), 1574 (w), 1514 (s), 1446 (s), 1394 (m), 1384 (m), 1330 (w), 1296 (w), 1260 (s), 1222 (w), 1172 (m), 1084 (s), 1046 (m), 1020 (m), 966 (m), 952 (m), 932 (m), 812 (m), 764 (m), 738 (m), 688 (m), 648 (w), 620 (w), 598 (w), 570 (w), 546 (w), 504 (w), 442 (w) cm^{-1}. Anal. Calcd for $C_{46}H_{49}BF_{15}N_5OSi_2W\cdot0.3CH_2Cl_2$: C, 44.5; H, 4.0; N, 5.6. Found: C, 44.5; H, 4.3; N, 5.6.

NMR Tube Scale Synthesis of [W(NPh){MeC(2-C$_5$H$_4$N)(CH$_2$NSiMe$_3$)(CH$_2$N(SiMe$_3$)C(O)NTol}-Me][MeBAr$^F_3$] (7-MeBAr$^F_3$). [W(NPh)(N_2N_{py})Me$_2$] (**1**) (23.3 mg, 0.038 mmol) was dissolved in CD_2Cl_2 (0.5 mL), and this solution was added to solid BAr$^F_3$ (19.3 mg, 0.038 mmol). The resulting brown solution was added to a J. Young NMR tube and cooled to −78 °C, and TolNCO (4.9 μL, 0.038 mmol) was added. The NMR tube was sealed and placed in a precooled NMR probe and analyzed in situ at −50 °C. ^{1}H NMR (CD_2Cl_2, 500.0 MHz, 223 K): 8.21 (1 H, t, H^4, $^3J(H^3H^4H^5) = 8.1$ Hz), 8.13 (1 H, d, H^6, $^3J(H^5H^6) = 5.6$ Hz), 7.82 (1 H, d, H^3, $^3J(H^3H^4) = 8.1$ Hz), 7.68 (2 H, t, *m*-C_6H_5, $^3J = 7.9$ Hz), 7.57 (1 H, t, H^5, $^3J(H^4H^5H^6) = 6.7$ Hz), 7.42 (2 H, d, *o*-C_6H_5, $^3J = 7.9$ Hz), 7.34 (1 H, t, *p*-C_6H_5, $^3J = 7.6$ Hz), 6.99 (2 H, d, *m*-4-C_6H_4Me, $^3J = 8.1$ Hz), 6.94 (2 H, d, *o*-4-C_6H_4Me, $^3J = 8.1$ Hz), 4.25 (1 H, d, C*H*HNSiMe$_3$, $^2J = 17.1$ Hz), 4.03 (1 H, d, CH*H*NSiMe$_3$, $^2J = 17.1$ Hz), 3.91 (1 H, d, C*H*HNCO, $^2J = 13.9$ Hz), 2.71 (1 H, d, CH*H*NCO, $^2J = 13.9$ Hz), 2.27 (3 H, s, 4-C_6H_4Me), 1.74 (3 H, s, *Me*CCH$_2$), 1.33 (3 H, s, WMe), 0.36 (12 H, br s, BMe and CH$_2$N(Si*Me*$_3$)CO), 0.28 (9 H, s, CH$_2$NSi*Me*$_3$) ppm. ^{13}C{^{1}H} NMR (CD_2Cl_2, 125.7 MHz, 223 K): 157.6 (C^2), 156.0 (CO), 148.6 (C^6), 147.7 (Ar^F, $^1J = 237$ Hz), 141.6 (C^4), 137.9 (Ar^F, $^1J = 242$ Hz), 136.9 (Ar^F, $^1J = 243$ Hz), 135.6 (*ipso*-4-C_6H_4Me), 135.0 (*p*-4-C_6H_4Me), 128.5 (*m*-C_6H_5), 128.3 (*p*-C_6H_5), 126.5 (*ipso*-C_6H_5), 125.2 (*o*-C_6H_5), 125.0 (C^5), 124.0 (*m*-4-C_6H_4Me), 122.9 (*o*-4-C_6H_4Me), 121.3 (C^3), 63.7 (*C*H$_2$SiMe$_3$), 51.4 (*C*(CH$_2$NSiMe$_3$)), 50.4 (*C*H$_2$NCO), 45.1 (WMe), 22.0 (*Me*CCH$_2$), 20.9 (4-C_6H_4Me), 9.5 (br, BMe), 1.5 (SiMe$_3$) ppm. ^{19}F NMR (CD_2Cl_2, 470.4 MHz, 223 K): −135.4 (6 F, d, *o*-Ar^F, $^3J = 23.0$ Hz), −167.4 (3 F, t, *p*-Ar^F, $^3J = 21.7$ Hz), −170.2 (6 F, app. t, *m*-Ar^F, app. $^3J = 21.3$ Hz) ppm. ^{11}B{^{1}H} NMR (CD_2Cl_2, 160.4 MHz, 223 K): −15.0 (BMe) ppm.

[W(NPh)(MeC(2-C$_5$H$_4$N)(CH$_2$NSiMe$_3$)(CH$_2$NC(OSiMe$_3$)-NTol)Me][MeBAr$^F_3$] (8-MeBAr$^F_3$). To a stirred solution of [W(NPh)(N_2N_{py})Me$_2$] (**1**) (200 mg, 0.32 mmol) in CH_2Cl_2 (20 mL) cooled to 0 °C was added a solution of BAr$^F_3$ (166 mg, 0.32 mmol) in CH_2Cl_2 (20 mL). To the stirred solution was added TolNCO (43 mg, 40 μL, 0.324 mmol). After stirring at room temperature for 1 h the solvent was removed under reduced pressure to afford **8-MeBAr$^F_3$** as a golden-brown solid in 260 mg (64%) yield. ^{1}H NMR (CD_2Cl_2, 500.0 MHz, 293 K): 8.65 (1 H, dd, H^6, $^3J(H^5H^6) = 5.9$ Hz, $^4J(H^3H^6) = 1.5$ Hz), 8.18 (1 H, td, H^4, $^3J(H^3H^4H^5) = 7.8$ Hz, $^4J(H^4H^6) = 1.5$ Hz), 7.83 (1 H, d, H^3, $^3J(H^3H^4) = 8.3$ Hz), 7.57−7.52 (3 H, overlapping m, H^5, *m*-C_6H_5), 7.29 (2 H, dd, *o*-C_6H_5, $^3J = 8.8$ Hz, $^4J = 1.5$ Hz), 7.24 (1 H, t, *p*-C_6H_5, $^3J = 7.8$ Hz), 7.02 (2 H, d, *m*-4-C_6H_4Me, $^3J = 7.8$ Hz), 6.89 (2 H, d, *o*-4-C_6H_4Me, $^3J = 8.3$ Hz), 4.21 (1 H, d, C*H*HNSiMe$_3$, $^2J = 16.1$ Hz), 4.03 (1 H, d, CH*H*NSiMe$_3$, $^2J = 16.6$ Hz), 3.62 (1 H, d, C*H*HNCOSiMe$_3$, $^2J = 12.2$ Hz), 3.12 (1 H, d, CH*H*NCOSiMe$_3$, $^2J = 12.2$ Hz), 2.25 (3 H, s, 4-C_6H_4Me), 1.69 (3 H, s, *Me*CCH$_2$), 1.21 (3 H, s, WMe, ^2J(WH) = 6.8 Hz (15%)), 0.45 (3 H, br s, BMe), 0.40 (9 H, s, NSiMe$_3$), 0.05 (9 H, s, OSiMe$_3$) ppm. ^{13}C{^{1}H} NMR (CD_2Cl_2, 125.7 MHz, 293 K): 161.2 (CO), 160.7 (C^2), 153.8 (*ipso*-C_6H_5), 149.2 (*o*-C_6H_5, ^1J(CH) = 168 Hz), 148.7 (C_6F_5, ^1J(CF) = 239 Hz), 142.2 (C^6, ^1J(CH) = 161 Hz), 138.5 (*ipso*-4-C_6H_4Me), 137.8 (C_6F_5, ^1J(CF) = 251 Hz), 136.7 (C_6F_5, ^1J(CF) = 251 Hz), 136.1 (*p*-4-C_6H_4Me), 130.4 (*o*-4-C_6H_4Me, ^1J(CH) = 172 Hz), 130.0 (*m*-C_6H_5, ^1J(CH) = 160 Hz), 129.0 (*p*-C_6H_5, ^1J(CH) =162 Hz), 127.1 (C,[4] ^1J(CH) = 159 Hz), 124.7 (*m*-4-C_6H_4Me, ^1J(CH) = 165 Hz), 123.8 (C^5, ^1J(CH) = 160 Hz), 121.9 (C^3, ^1J(CH) = 164 Hz), 64.6 (*C*H$_2$NSiMe$_3$, ^1J(CH) = 138 Hz), 54.6 (*C*H$_2$NCOSiMe$_3$, ^1J(CH) = 134 Hz), 51.2 ((*C*(CH$_2$NSiMe$_3$)$_2$), 43.1 (WMe, ^1J(CH) = 125 Hz, ^1J(WC) = 93 Hz (15%)), 21.4 (*Me*CCH$_2$, ^1J(CH) = 128 Hz), 20.9 (4-C_6H_4Me, ^1J(CH) = 128 Hz), 10.5 (BMe, ^1J(CH) = 116 Hz), 1.9 (NSiMe$_3$, ^1J(CH) = 125 Hz), −0.2 (OSiMe$_3$, ^1J(CH) = 118 Hz) ppm. ^{19}F NMR (CD_2Cl_2, 282.2 MHz, 293 K): −133.4 (6 F, d, *o*-Ar^F, $^3J = 19.8$ Hz), −165.6 (6 F, app. t, *p*-Ar^F, app. $^3J = 19.8$ Hz), −168.1 (3 F, t, *m*-Ar^F, $^3J = 22.7$ Hz) ppm. ^{11}B-{^{1}H} NMR (CD_2Cl_2, 160.4 MHz, 293 K): −14.7 (br s, MeBAr$^F_3$) ppm. IR (KBr pellet): 2960 (m), 2906 (m), 2856 (w), 2274 (w), 1640 (m), 1608 (m), 1568 (w), 1510 (s), 1484 (s), 1454 (s), 1384 (w), 1356 (m), 1296 (s), 1260 (s), 1170 (w), 1132 (w), 1086 (s), 1044 (w), 1030 (w), 1018 (w), 980 (m), 952 (m), 932 (w), 840 (s), 810 (m), 762 (m), 738 (w), 688 (w), 660 (w), 646 (w), 622 (w), 604 (w), 572 (w), 512 (w) cm^{-1}. Anal. Calcd for $C_{49}H_{47}BF_{15}N_5OSi_2W$: C, 46.8; H, 3.8; N, 5.6. Found: C, 46.4; H, 3.4; N, 5.4.

[W(NPh)(MeC(2-C$_5$H$_4$N)(CH$_2$NSiMe$_3$)(CH$_2$NC(OSiMe$_3$)-NPh)Me][MeBAr$^F_3$] (9-MeBAr$^F_3$). To a stirred solution of [W(NPh)($N_2^{TMS}N_{py}$)Me$_2$] (**1**) (200 mg, 0.32 mmol) in CH_2Cl_2 (20 mL) cooled to 0 °C was added a solution of BAr$^F_3$ (166 mg, 0.32 mmol) in CH_2Cl_2 (20 mL) followed by PhNCO (38 mg, 35 μL, 0.324 mmol). After stirring at room temperature for 1 h the solvent was removed under reduced pressure to afford **9-MeBAr$^F_3$** as a golden-brown solid. Yield: 280 mg (69%). ^{1}H NMR (CD_2Cl_2, 500.0 MHz, 293 K): 8.66 (1 H, dd, H^6, $^3J(H^5H^6) = 5.6$ Hz, $^4J(H^3H^6) = 1.2$ Hz), 8.19 (1 H, td, H^4, $^3J(H^3H^4H^5) = 8.0$ Hz, $^4J(H^4H^6) = 1.7$ Hz), 7.84 (1 H, d, H^3, $^3J(H^3H^4) = 8.0$ Hz), 7.58−7.52 (3 H, overlapping m, H^5, *m*-$C_6H_{5,imide}$), 7.29 (2 H, dd, *o*-$C_6H_{5,imide}$, $^3J = 8.3$ Hz, $^4J = 1.2$ Hz), 7.25−7.20 (3 H, overlapping m, *m*-Me$_3$SiOCNC$_6H_5$, *p*-$C_6H_{5,imide}$), 7.10 (1 H, t, *p*-Me$_3$SiOCNC$_6H_5$, $^3J = 7.6$ Hz), 6.81 (2 H, d, *o*-Me$_3$SiOCNC$_6H_5$, $^3J = 8.3$ Hz), 4.22 (1 H, d, C*H*HNSiMe$_3$, $^2J = 16.1$ Hz), 4.04 (1 H, d, CH*H*NSiMe$_3$, $^2J = 16.3$ Hz), 3.63 (1 H, d, C*H*HNCO-SiMe$_3$, $^2J = 12.0$ Hz), 3.14 (1 H, d, CH*H*NCOSiMe$_3$, $^2J = 12.2$ Hz), 1.70 (3 H, s, *Me*CCH$_2$), 1.23 (3 H, s, WMe, ^2J(WH) = 6.5 Hz (15%)), 0.45 (3 H, br s, BMe), 0.40 (9 H, s, NSiMe$_3$), −0.09 (9 H, s, OSiMe$_3$) ppm. ^{13}C NMR (CD_2Cl_2, 125.7 MHz, 293 K): 161.2 (CO), 160.7 (C^2), 153.8 (*ipso*-$C_6H_{5,imide}$), 149.2 (*o*-$C_6H_{5,imide}$, ^1J(CH) = 161 Hz), 148.7 (C_6F_5, ^1J(CF) = 239 Hz), 142.2 (C^6, ^1J(CH) = 166 Hz), 141.1 (*ipso*-Me$_3$SiOCNC$_6H_5$), 137.8 (C_6F_5, ^1J(CF) = 251 Hz), 136.7 (C_6F_5, ^1J(CF) = 251 Hz), 129.6 (*o*-Me$_3$SiOCNC$_6H_5$, ^1J(CH) = 159 Hz), 129.5 (*m*-Me$_3$SiOCNC$_6H_5$, ^1J(CH) = 160 Hz), 128.9 (*o*-$C_6H_{5,imide}$, ^1J(CH) = 161 Hz), 127.1 (C,[4] ^1J(CH) = 163 Hz), 126.0 (*m*-$C_6H_{5,imide}$, ^1J(CH) = 161 Hz), 124.8 (*p*-Me$_3$SiOCNC$_6H_5$, ^1J(CH) = 162 Hz), 123.9 (C,[5] ^1J(CH) = 159 Hz), 122.0 (C^3, ^1J(CH) = 165 Hz), 64.6 (*C*H$_2$NSiMe$_3$, ^1J(CH) = 137 Hz), 54.6 (*C*H$_2$NCOSiMe$_3$, ^1J(CH) = 136 Hz), 51.2 (*C*(CH$_2$NSiMe$_3$)$_2$), 43.1 (WMe, ^1J(CH) = 123 Hz), 21.4 (*Me*CCH$_2$, ^1J(CH) = 128 Hz), 10.5 (BMe), 1.9 (NSiMe$_3$, ^1J(CH)

= 120 Hz), −0.2 ($OSiMe_3$, ^1J(CH) = 122 Hz) ppm. ^{19}F NMR (CD_2Cl_2, 282.2 MHz, 293 K): −133.4 (6 F, d, *o*-Ar^F, ^3J = 19.8 Hz), −165.6 (6 F, app. t, *p*-Ar^F, app. ^3J = 19.8 Hz), −168.1 (3 F, t, *m*-Ar^F, ^3J = 22.7 Hz) ppm. ^{11}B{^{1}H} NMR (CD_2Cl_2, 160.4 MHz, 293 K): −14.7 (br s, $MeBAr^F_3$) ppm. IR (KBr pellet): 3064 (w), 2958 (m), 2908 (m), 2856 (m), 2262 (w), 1948 (w), 1642 (s), 1608 (s), 1596 (m), 1584 (m), 1510 (s), 1454 (w), 1382 (w), 1358 (m), 1296 (m), 1258 (s), 1086 (s), 1046 (m), 1020 (m), 980 (s), 834 (m), 788 (m), 688 (w), 660 (w), 646 (w), 604 (w), 594 (w), 538 (w), 474 (w), 444 (w), 420 (w), 406 (w) cm^{-1}. Anal. Calcd for $C_{48}H_{45}BF_{15}N_5OSi_2W$: C, 45.8; H, 3.7; N, 5.6. Found: C, 46.3; H, 3.7; N, 5.4.

Preparation of [W(NPh)(MeC(2-C_5H_4N)(CH_2NSiMe_3)-(CH_2NC(SSiMe_3)N^{t}Bu)Me][$MeBAr^F_3$] (10-$MeBAr^F_3$). To a stirred solution of [W(NPh)(N_2N_{py})Me_2] (**1**) (150 mg, 0.24 mmol) in CH_2Cl_2 (20 mL) cooled to 0 °C was added a solution of BAr^F_3 (125 mg, 0.24 mmol) in CH_2Cl_2 (20 mL) followed by ^{t}BuNCS (28 mg, 31 μL, 0.243 mmol). After stirring at room temperature for 1 h the volatiles were removed under reduced pressure to afford **10-$MeBAr^F_3$** as a golden-brown solid. Yield: 157 mg (52%). ^{1}H NMR (CD_2Cl_2, 500.0 MHz, 293 K): 9.01 (1 H, dd, H^6, ^3J(H^5H^6) = 5.8 Hz, ^4J(H^4H^6) = 1.2 Hz), 8.12 (1 H, td, H^4, ^3J($H^3H^4H^5$) = 7.8 Hz, ^4J(H^4H^6) = 1.5 Hz), 7.74 (1 H, d, H^3, ^3J(H^3H^4) = 8.1 Hz), 7.66−7.56 (3 H, overlapping m, H^5, *m*-C_6H_5), 7.40−7.33 (3 H, overlapping m, *o*-C_6H_5, *p*-C_6H_5), 4.70 (1 H, d, C*H*HNSiMe_3, ^2J = 13.5 Hz), 4.06 (1 H, d, C*H*HNCO-SiMe_3, ^2J = 16.8 Hz), 3.90 (1 H, d, CH*H*NCOSiMe_3, ^2J = 16.8 Hz), 2.55 (1 H, d, CH*H*NSiMe_3, ^2J = 13.5 Hz), 1.70 (3 H, s, *Me*CCH_2), 1.40 (9 H, s, CMe_3), 1.36 (3 H, s, WMe, ^2J(WH) = 7.3 Hz (15%)), 0.43 (3 H, br s, BMe), 0.37 (9 H, s, $OSiMe_3$), 0.32 (9 H, s, $NSiMe_3$) ppm. ^{13}C NMR (CD_2Cl_2, 125.7 MHz, 293 K): 160.1 (C^2), 153.1 (CS), 152.9 (*ipso*-C_6H_5), 148.7 (C_6F_5, ^1J(CF) = 239 Hz), 141.9 (C^6, ^1J(CH) = 166 Hz), 137.8 (C_6F_5, ^1J(CF) = 251 Hz), 136.7 (C_6F_5, ^1J(CF) = 251 Hz), 130.1 (*o*-C_6H_5, ^1J(CH) = 156 Hz), 129.4 (*m*-C_6H_5, ^1J(CH) = 162 Hz), 127.5 (*p*-C_6H_5, ^1J(CH) = 157 Hz), 125.3 (C,[4] ^1J(CH) = 160 Hz), 121.1 (C,[5] ^1J(CH) = 165 Hz), 119.7 (C^3, ^1J(CH) = 167 Hz), 64.7 (CH_2NSiMe_3, ^1J(CH) = 140 Hz), 55.5 ($CH_2NCOSiMe_3$, ^1J(CH) = 137 Hz), 54.8 (CMe_3), 51.7 ($C(CH_2NSiMe_3)_2$), 43.4 (WMe, ^1J(CH) = 126 Hz), 30.7 (CMe_3, ^1J(CH) = 128 Hz), 22.9 (*Me*CCH_2, ^1J(CH) = 126 Hz), 10.5 (BMe), 1.4 ($NSiMe_3$, ^1J(CH) = 120 Hz), 0.0 ($OSiMe_3$, ^1J(CH) = 123 Hz) ppm. ^{19}F NMR (CD_2Cl_2, 282.2 MHz, 293 K): −133.4 (6 F, d, *o*-Ar^F, ^3J = 19.8 Hz), −165.6 (6 F, app. t, *p*-Ar^F, app. ^3J = 19.8 Hz), −168.1 (3 F, t, *m*-Ar^F, ^3J = 22.7 Hz) ppm. ^{11}B{^{1}H} NMR (CD_2Cl_2, 160.4 MHz, 293 K): −14.7 (br s, $MeBAr^F_3$) ppm. IR (KBr pellet): 3396 (w), 3066 (w), 2970 (m), 2904 (m), 2850 (w), 2100 (br m), 1966 (w), 1644 (s), 1608 (m), 1552 (m), 1510 (s), 1482 (s), 1454 (s), 1382 (w), 1354 (w), 1298 (w), 1258 (s), 1200 (s), 1172 (w), 1088 (s), 1044 (w),1020 (w), 966 (s), 952 (m), 934 (m), 836 (s), 812 (w), 782 (w), 722 (w), 686 (w), 660 (w), 644 (w), 570 (w), 484 (w), 442 (w), 428 (w), 402 (w) cm^{-1}. Anal. Calcd for $C_{46}H_{49}BF_{15}N_5SSi_2W$: C, 44.5; H, 4.0; N, 5.7. Found: C, 44.2; H, 4.1; N, 5.6.

[W(NPh){MeC(2-C_5H_4N)(CH_2NSiMe_3)(CH_2N(SiMe_3)C-(NAr)O}Me] [$MeBAr^F_3$] (11-$MeBAr^F_3$). To a stirred solution of [W(NPh)(N_2N_{py})Me_2] (**1**) (200 mg, 0.324 mmol) in CH_2Cl_2 was added a solution of BAr^F_3 (166 mg, 0.324 mmol) in CH_2Cl_2 (10 mL). The resulting brown solution was stirred for 1 min before cooling to −78 °C. To the cold reaction was added 2,6-diisopropylphenyl isocyanate (69.3 μL, 65.9 mg, 0.324 mmol). The mixture was again stirred for 1 h before warming to −30 °C and concentrating to ca. 10 mL under reduced pressure. Cold (−30 °C) pentane (30 mL) was added, which caused a brown oil to separate from the solution, which was washed with pentane (3 × 5 mL) and dried in vacuo to yield **11-$MeBAr^F_3$** as a brown solid. Yield: 207 mg (48%). The compound was also prepared and analyzed in situ by reaction with [W(NPh)(N_2N_{py})Me][$MeBAr^F_3$] prepared in CD_2Cl_2 in a J. Young NMR tube and cooled to −78 °C. To this was added 2,6-diisopropylphenyl isocyanate (3 mg, 3.2 μL, 0.03 mmol) also at −78 °C. The mixture was analyzed by NMR spectroscopy in a precooled NMR probe at −30 °C. On warming to room temperature, quantitative conversion to **12-$MeBAr^F_3$** was observed after 4 h. ^{1}H NMR (CD_2Cl_2, 500.0 MHz, 293 K): 8.56 (1 H, dd, H^6, ^3J(H^5H^6) = 5.8 Hz, ^4J(H^4H^6) = 1.1 Hz), 8.27 (1 H, td, H^4, ^3J($H^3H^4H^5$) = 7.8 Hz, ^4J(H^4H^6) = 1.4 Hz), 7.89 (1 H, d, H^3, ^3J(H^3H^4) = 8.1 Hz), 7.65 (2 H, t, *m*-C_6H_5, ^3J = 8.0 Hz), 7.56 (1 H, t, H^5, ^3J($H^4H^5H^6$) = 7.1 Hz), 7.34 (2 H, d, *o*-C_6H_5, ^3J = 7.6 Hz), 7.19 (1 H, t, *p*-C_6H_5, ^3J = 7.5 Hz), 7.00−6.94 (3 H, overlapping m, 2,6-$C_6H_3{}^iPr_2$), 4.39 (1 H, d, C*H*HNSiMe_3 "out", ^2J = 16.7 Hz), 4.18 (1 H, d, C*H*HNCO "out", ^2J = 14.3 Hz), 4.13 (1 H, d, CH*H*NSiMe_3 "in", ^2J = 16.7 Hz), 3.08 (1 H, d, CH*H*NCO "in", ^2J = 14.3 Hz), 1.75 (3 H, s, $MeCCH_2$), 1.69 (2 H, br s, C*H*Me_2), 1.37 (3 H, s, WMe, ^2J(WH) = 8.0 Hz), 1.01 (6 H, d, CH*Me*$_2$, ^3J = 6.8 Hz), 0.85 (6 H, d, CH*Me*$_2$, ^3J = 6.8 Hz), 0.47 (9 H, s, CH_2N(Si*Me*$_3$)CO), 0.45 (3 H, br s, BMe), 0.41 (9 H, s, CH_2NSiMe_3) ppm. ^{13}C{^{1}H} NMR (CD_2Cl_2, 125.7 MHz, 243 K): 159.2 (C^2, C═O), 152.0 (*ipso*-C_6H_5), 149.6 (C^6), 148.0 (Ar^F, ^1J(CF) = 238 Hz), 143.0 (C^4), 138.0 (*o*-2,6-$C_6H_3{}^iPr_2$), 137.9 (Ar^F, ^1J(CF) = 242 Hz), 136.9 (Ar^F, ^1J(CF) = 244 Hz), 130.1 (*o*-C_6H_5), 129.3 (*ipso*-2,6-$C_6H_3{}^iPr_2$), 129.2 (*m*-C_6H_5), 126.1 (*p*-C_6H_5), 125.7 (C^5), 124.2 (*p*-2,6-$C_6H_3{}^iPr_2$), 122.7 (br, *m*-$C_6H_3{}^i$-Pr_2), 120.8 (C^3), 64.3 (CH_2NSiMe_3), 56.9 (CH_2NCO), 51.9 ($C(CH_2NSiMe_3)$), 46.9 (WMe), 27.9 ($CHMe_2$), 22.5 (CH*Me*$_2$), 22.3 (CH*Me*$_2$), 1.3 (CH_2NSiMe_3), −0.9 (CH_2N(Si*Me*$_3$)CO) ppm. ^{19}F NMR (CD_2Cl_2, 470.4 MHz, 243 K): −135.2 (6 F, d, *o*-Ar^F, ^3J = 21.5 Hz), −167.7 (3 F, t, *p*-Ar^F, ^3J = 21.8 Hz), −170.4 (6 F, app. t, *m*-Ar^F, app. ^3J = 20.2 Hz) ppm. ^{11}B{^{1}H} NMR (CD_2Cl_2, 160.4 MHz, 243 K): −14.9 (BMe) ppm. IR (KBr pellet): 2962 (s), 2872 (w), 1690 (m, $\nu_{C=N}$), 1640 (m), 1608 (m), 1574 (m), 1570 (s), 1454 (s), 1384 (m), 1356 (m), 1326 (w), 1298 (w), 1260 (w), 1212 (w), 1084 (s), 1022 (w), 966 (s), 952 (s), 934 (m), 840 (s), 804 (s), 804 (m), 762 (m), 736 (w), 686 (w), 660 (w), 644 (w), 594 (w), 570 (w), 556 (w), 512 (w), 464 (w), 422 (w) cm^{-1}. Anal. Calcd for $C_{54}H_{57}BF_{15}N_5OSi_2W\cdot0.5CH_2Cl_2$: C, 47.8; H, 4.3; N, 5.1. Found: C, 47.7; H, 4.3; N, 5.3.

[W(NPh){MeC(2-C_5H_4N)(CH_2NSiMe_3)(CH_2NC{N(SiMe_3)-Ar}O}Me] [$MeBAr^F_3$] (12-$MeBAr^F_3$). To a stirred solution of [W(NPh)(N_2N_{py})Me_2] (**1**) (200 mg, 0.324 mmol) in CH_2Cl_2 (10 mL) was added a solution of BAr^F_3 (166 mg, 0.324 mmol) in CH_2Cl_2 (10 mL). The resulting brown solution was allowed to stir for 1 min before adding a solution of 2,6-diisopropylphenyl isocyanate (66 mg) in CH_2Cl_2 (5 mL). The solution was allowed to stir for 18 h before concentrating to ca. 5 mL. The product was precipitated from the solution by the addition of pentane (30 mL), which afforded a brown oil. The supernatant was decanted and the oil dried in vacuo to afford **12-$MeBAr^F_3$** as a brown solid. Yield: 185 mg (43%). ^{1}H NMR (CD_2Cl_2, 500.0 MHz, 293 K): 8.89 (1 H, d, H^6, ^3J(H^5H^6) = 5.9 Hz), 8.18 (1 H, td, H^4, ^3J($H^3H^4H^5$) = 7.8 Hz, ^4J(H^4H^6) = 1.5 Hz), 7.71 (2 H, overlapping m, H^3 and H^5), 7.61 (2 H, t, *m*-C_6H_5, ^3J = 8.3 Hz), 7.34 (3 H, overlapping m, *o*-C_6H_5 and *p*-2,6-$C_6H_3{}^iPr_2$), 7.26 (2 H, overlapping m, *p*-C_6H_5 and *m*-2,6-$C_6H_3{}^iPr_2$ "in"), 7.10 (1 H, dd, *m*-2,6-$C_6H_3{}^iPr_2$ "out", ^3J = 7.8 Hz, ^4J = 1.5 Hz), 4.20 (1 H, d, C*H*HNSiMe_3 "out", ^2J = 15.6 Hz), 3.85 (1 H, d, CH*H*NSiMe_3 "in", ^2J = 15.6 Hz), 2.80 (1 H, sept, C*H*Me_2 "in", ^3J = 6.8 Hz), 2.75 (1 H, d, C*H*HNCO "out", ^2J = 13.2 Hz), 2.45 (1 H, d, CH*H*NCO "in", ^2J = 13.2 Hz), 2.11 (1 H, sept, C*H*Me_2 "out", ^3J = 6.8 Hz), 1.36 (6 H, s, WMe and *Me*C(CH_2NSiMe_3), ^2J(WH) = 7.2 Hz), 1.30 (3 H, d, CH*Me*$_2$ "in, back", ^3J = 6.8 Hz), 1.09 (3 H, d, CH*Me*$_2$ "in, forward", ^3J = 6.8 Hz), 1.04 (3 H, d, CH*Me*$_2$ "out, forward", ^3J = 6.8 Hz), 0.48 (3 H, d, CH*Me*$_2$ "out, back", ^3J = 6.8 Hz), 0.45 (3 H, br s, BMe), 0.36 (9 H, s, CH_2NSiMe_3), 0.06 (9 H, s, $OCNSiMe_3$) ppm. ^{13}C{^{1}H} NMR (CD_2Cl_2, 125.7 MHz, 293 K): 169.2 (O*C*N-2,6-$C_6H_3{}^iPr_2$), 159.8 (C^2), 153.6 (*ipso*-C_6H_5), 148.8 (Ar^F, ^1J(CF) = 240 Hz), 148.5 (C^6), 145.7 (*o*-2,6-$C_6H_3{}^iPr_2$ "in"), 144.7 (*o*-2,6-$C_6H_3{}^iPr_2$ "out"), 141.9 (C^4), 137.9 (Ar^F, ^1J(CF) = 242 Hz), 136.9 (Ar^F, ^1J(CF) = 244 Hz), 133.0 (*ipso*-$C_6H_3{}^iPr_2$), 129.6 (*o*-C_6H_5), 129.3 (*p*-C_6H_5), 128.9 (*m*-C_6H_5), 127.0 (*p*-2,6-$C_6H_5{}^iPr_2$), 125.9 (*m*-2,6-$C_6H_3{}^iPr_2$ "in"), 125.1 (C^5), 124.9 (*m*-2,6-$C_6H_3{}^iPr_2$ "out"), 122.9 (C^3), 65.2 (CH_2-$NSiMe_3$), 53.8 ($C(CH_2NSiMe_3)$), 50.6 (CH_2NCO), 45.2 (WMe,

^1J(WC) = 93 Hz), 28.9 (*C*HMe$_2$), 28.8 (*C*HMe$_2$), 25.3 (*C*HMe$_2$ "in, forward"), 24.7 (*C*HMe$_2$ "out, back"), 24.1 (*C*HMe$_2$ "in, back"), 23.3 (*C*HMe$_2$ "out, forward"), 21.1 (*Me*C(CH$_2$NSiMe$_3$)), 10.4 (br, BMe), 1.7 (CH$_2$NSi*Me*$_3$), 0.0 (OCNSi*Me*$_3$) ppm. ^{19}F NMR (CD$_2$Cl$_2$, 470.4 MHz, 293 K): −135.0 (6 F, d, *o*-Ar^F, ^3J = 21.1 Hz), −168.5 (3 F, t, *p*-Ar^F, ^3J = 21.1 Hz), −171.2 (6 F, app. t, *m*-Ar^F, app. ^3J = 21.1 Hz) ppm. ^{11}B{^{1}H} NMR (CD$_2$Cl$_2$, 160.4 MHz, 293 K): −14.7 (BMe) ppm. IR (KBr pellet): 2966 (m), 2906 (w), 2874 (w), 1640 (m), 1608 (m), 1590 (w), 1510 (s), 1482 (m), 1456 (s), 1404 (m), 1384 (m), 1356 (m), 1326 (w), 1296 (m), 1258 (s), 1086 (s), 1022 (w), 992 (m), 966 (m), 952 (m), 934 (m), 894 (w), 838 (s), 804 (m), 784 (w), 764 (m), 738 (w), 708 (w), 688 (w), 594 (w), 570 (w), 512 (w), 418 (w), 408 (w) cm^{-1}. Anal. Calcd for C$_{54}$H$_{57}$BF$_{15}$N$_5$OSi$_2$W·CH$_2$Cl$_2$: C, 46.8; H, 4.2; N, 5.0. Found: C, 46.6; H, 4.3; N, 5.3.

Nb(N^{t}Bu){MeC(2-C$_5$H$_4$N)(CH$_2$NSiMe$_3$)(CH$_2$NC(OSiMe$_3$)-N^{t}Bu)}Cl (15). To a stirred solution of [Nb(N^{t}Bu)(N$_2$N$_{py}$)Cl(py)] (260 mg, 0.444 mmol) in CH$_2$Cl$_2$ (20 mL) was added ^{t}BuNCO (51 μL, 0.444 mmol). The yellow solution was stirred for 3 h at room temperature. The volatiles were removed under reduced pressure to afford a yellow powder, which was extracted into pentanes and filtered. The volatiles were removed under reduced pressure to afford **15** as a pale yellow powder. Yield: 150 mg (55%). Diffraction quality crystals were grown by slow evaporation of a pentane solution at room temperature over 2 days. ^{1}H NMR (CD$_2$Cl$_2$, 500.0 MHz, 293 K): 9.29 (1 H, dd, H^6, ^3J(H^{5}H^6) = 5.4 Hz, ^4J(H^{4}H^6) = 1.9 Hz), 7.81 (1 H, td, H^4, ^3J(H^{4}H^{5}H^6) = 7.8 Hz, ^4J(H^{4}H^6) = 1.9 Hz), 7.44 (1 H, d, H^3, ^3J(H^{3}H^4) = 7.8 Hz), 7.27 (1 H, m, H^5), 3.52 (1 H, d, C*H*HNSiMe$_3$, ^2J = 13.7 Hz), 3.29 (1 H, d, C*H*HNCOSiMe$_3$, ^2J = 11.7 Hz), 3.19 (1 H, d, CH*H*NSiMe$_3$, ^2J = 13.7 Hz), 2.89 (1 H, d, CH*H*NCOSiMe$_3$, ^2J = 11.7 Hz), 1.39 (3 H, s, *Me*C(CH$_2$N)$_2$), 1.31 (9 H, s, CMe$_{3,imide}$), 1.17 (9 H, s, CMe$_{3,amide}$), 0.31 (9 H, s, NSiMe$_3$), 0.20 (9 H, s, OSiMe$_3$) ppm. ^{13}C{^{1}H} NMR (CD$_2$Cl$_2$, 125.7 MHz, 293 K): 163.8 (C^2), 156.8 (CO), 150.6 (C^6), 138.9 (C^4), 121.6 (C^5), 120.6 (C^3), 65.9 (*C*Me$_{3,imide}$), 62.9 (*C*H$_2$NSiMe$_3$), 54.7 (*C*H$_2$NCOSiMe$_3$), 52.0 (*C*Me$_{3,amide}$), 51.3 (Me*C*(CH$_2$N)$_2$), 32.4 (C*Me*$_{3,imide}$), 31.6 (C*Me*$_{3,amide}$), 22.7 (*Me*C(CH$_2$N)$_2$), 2.4 (NSiMe$_3$), 1.0 (OSiMe$_3$) ppm. IR (KBr pellet): 2968 (s), 2356 (w), 1867 (w), 1842 (w), 1824 (w), 1651 (m), 1601 (m), 1573 (m), 1524 (s), 1479 (w), 1470 (m), 1455 (w), 1427 (s), 1391 (m), 1377 (w), 1356 (m), 1338 (w), 1321 (w), 1296 (w), 1245 (s), 1225 (m), 1160 (m), 1134 (w), 1127 (w), 1090 (w), 1060 (m), 1051 (w), 1020 (m), 1012 (w), 976 (m), 924 (m), 900 (w), 844 (s), 796 (w), 786 (w), 758 (m), 738 (w), 717 (w), 689 (w), 673 (m), 640 (w), 618 (w), 598 (w), 565 (m), 485 (w), 470 (w), 451 (w), 431 (w), 408 (w) cm^{-1}. High-resolution EI mass spectrum for [Nb(N^{t}Bu){MeC(2-C$_5$H$_4$N)(CH$_2$NSiMe$_3$)(CH$_2$NC(OSiMe$_3$)N^{t}Bu)}Cl]$^+$: Found (calculated for C$_{24}$H$_{47}$ClN$_5$NbOSi$_2$): *m/z* = 605.2083 (605.2071). Anal. Calcd for C$_{24}$H$_{47}$ClN$_5$NbOSi$_2$: C, 47.5; H, 7.8; N, 11.6. Found: C, 47.0; H, 8.1; N, 11.6.

Ta(N^{t}Bu){MeC(2-C$_5$H$_4$N)(CH$_2$NSiMe$_3$)(CH$_2$NC(OSiMe$_3$)-N^{t}Bu)}Cl (16). To a stirred solution of [Ta(N^{t}Bu)(N$_2$N$_{py}$)Cl(py)] (230 mg, 0.341 mmol) in CH$_2$Cl$_2$ (20 mL) was added ^{t}BuNCO (39 μL, 0.341 mmol). The yellow solution was stirred for 3 h at room temperature. The volatiles were removed under reduced pressure to afford a yellow powder, which was extracted into pentanes and filtered. The volatiles were removed under reduced pressure to afford **16** as a pale yellow powder. Yield: 110 mg (46%). ^{1}H NMR (CD$_2$Cl$_2$, 300.0 MHz, 293 K): 9.33 (1 H, dd, H^6, ^3J(H^{5}H^6) = 5.3 Hz, ^4J(H^{4}H^6) = 1.8 Hz), 7.80 (1 H, m, H^4), 7.45 (1 H, d, H^3, ^3J(H^{3}H^4) = 7.6 Hz), 7.28 (1 H, m, H^5), 3.63 (1 H, d, C*H*HNSiMe$_3$, ^2J = 13.5 Hz), 3.43 (1 H, d, C*H*HNCOSiMe$_3$, ^2J = 11.7 Hz), 3.40 (1 H, d, CH*H*NSiMe$_3$, ^2J = 13.5 Hz), 2.96 (1 H, d, CH*H*NCOSiMe$_3$, ^2J = 11.7 Hz), 1.38 (3 H, s, *Me*C(CH$_2$N)$_2$), 1.30 (9 H, s, CMe$_{3,imide}$), 1.21 (9 H, s, CMe$_{3,amide}$), 0.32 (9 H, s, NSiMe$_3$), 0.24 (9 H, s, OSiMe$_3$) ppm. ^{13}C{^{1}H} NMR (CD$_2$Cl$_2$, 75.5 MHz, 293 K): 163.8 (C^2), 156.7 (CO), 150.6 (C^6), 139.0 (C^4), 121.8 (C^5), 120.5 (C^3), 64.1 (*C*Me$_{3,imide}$), 61.8 (*C*H$_2$NSiMe$_3$), 54.2 (*C*H$_2$NCOSiMe$_3$), 51.6 (CMe$_{3,amide}$), 51.5 (Me*C*(CH$_2$N)$_2$), 34.1 (C*Me*$_{3,imide}$), 31.6 (C*Me*$_{3,amide}$), 22.6 (*Me*C(CH$_2$N)$_2$), 2.5 (NSiMe$_3$), 0.9 (OSiMe$_3$) ppm. IR (KBr pellet): 3303 (m), 2966 (s), 2898 (m), 2744 (w), 2719 (w), 2106 (w), 1868 (w), 1651 (m), 1603 (m), 1573 (m), 1520 (s), 1472 (s), 1455 (m), 1432 (s), 1391 (m), 1375 (w), 1355 (m), 1337 (w), 1326 (w), 1272 (s), 1244 (s), 1214 (w), 1168 (m), 1140 (w), 1092 (w), 1063 (s), 1022 (m), 1012 (m), 978 (m), 927 (s), 844 (s), 797 (w), 786 (w), 756 (m), 718 (w), 670 (m), 640 (w), 618 (w), 595 (w), 564 (m), 545 (w) cm^{-1}. High-resolution EI mass spectrum: Found (calculated for C$_{24}$H$_{46}$ClN$_5$OSi$_2$Ta−H): *m/z* = 692.2430 (692.2410). Anal. Calcd for C$_{24}$H$_{47}$ClN$_5$OSi$_2$Ta: C, 41.5; H, 6.8; N, 10.1. Found: C, 41.5; H, 6.6; N, 10.0.

Nb(N^{t}Bu){MeC(2-C$_5$H$_4$N)(CH$_2$NSiMe$_3$)(CH$_2$NC(OSiMe$_3$)-NTol)}Cl (17). To a stirred solution of [Nb(N^{t}Bu)(N$_2$N$_{py}$)Cl(py)] (200 mg, 0.341 mmol) in CH$_2$Cl$_2$ (20 mL) was added TolNCO (43 μL, 0.341 mmol). After stirring for 3 h at room temperature the volatiles were removed under reduced pressure to afford **17** as a yellow powder. Yield: 115 mg (52%). ^{1}H NMR (CD$_2$Cl$_2$, 500.0 MHz, 293 K): 9.36 (1 H, d, H^6, ^3J(H^{5}H^6) = 5.4 Hz), 7.83 (1 H, m, H^4), 7.52 (1 H, d, H^3, ^3J(H^{3}H^4) = 8.3 Hz), 7.29 (1 H, m, H^5), 7.05 (4 H, m, NC$_6$*H*$_4$Me), 3.60 (1 H, d, C*H*HNSiMe$_3$, ^2J = 13.7 Hz), 3.47 (1 H, d, C*H*HNCOSiMe$_3$, ^2J = 11.7 Hz), 3.30 (1 H, d, CH*H*NSiMe$_3$, ^2J = 13.7), 3.02 (1 H, d, CH*H*NCOSiMe$_3$, ^2J = 11.7 Hz), 2.25 (3 H, s, NC$_6$H$_4$*Me*), 1.46 (3 H, s, *Me*C(CH$_2$N)$_2$), 1.09 (9 H, s, CMe$_3$), 0.33 (9 H, s, NSiMe$_3$), −0.28 (9 H, s, OSiMe$_3$) ppm. ^{13}C{^{1}H} NMR (CD$_2$Cl$_2$, 125.7 MHz, 293 K): 163.5 (C^2), 155.7 (CO), 150.3 (C^6), 143.5 (*p*-C$_6$H$_4$Me), 139.2 (C^4), 131.4 (*i*-C$_6$H$_4$Me), 129.3 (*m*-C$_6$H$_4$Me), 123.2 (*o*-C$_6$H$_4$Me), 122.5 (C^5), 121.1 (C^3), 66.8 (*C*Me$_3$), 63.3 (CH$_2$NSiMe$_3$), 53.2 (CH$_2$NCOSiMe$_3$), 51.2 (Me*C*(CH$_2$N)$_2$), 31.8 (C*Me*$_3$), 22.9 (*Me*C(CH$_2$N)$_2$), 20.9 (C$_6$H$_4$*Me*), 2.1 (NSiMe$_3$), 0.1 (OSiMe$_3$) ppm. IR (KBr pellet): 3316 (w), 3109 (w), 3072 (w), 2968 (s), 2921 (m), 2894 (m), 2854 (m), 2752 (w), 2655 (w), 2592 (w), 2332 (w), 2161 (w), 2095 (w), 2002 (w), 1968 (w), 1923 (w), 1891 (w), 1868 (w), 1830 (w), 1792 (w), 1772 (w), 1749 (w), 1733 (w), 1716 (w), 1696 (w), 1684 (w), 1652 (w), 1636 (w), 1601 (s), 1572 (m), 1558 (w), 1510 (s), 1505 (s), 1468 (s), 1447 (m), 1438 (m), 1407 (m), 1379 (w), 1356 (m), 1333 (m), 1312 (w), 1284 (s), 1245 (s), 1216 (m), 1179 (w), 1165 (w), 1141 (w), 1122 (s), 1089 (m), 1061 (s), 1053 (s), 1023 (s), 1012 (m), 972 (m), 926 (s), 879 (m), 844 (s), 790 (w), 761 (m), 754 (m), 739 (w), 688 (w), 666 (m), 642 (w), 622 (w), 592 (w), 572 (m), 555 (w), 549 (w), 529 (w), 515 (w) cm^{-1}. EI mass spectrum: *m/z* = 624 (5%) [M − Me]$^+$. Anal. Calcd for C$_{27}$H$_{45}$ClN$_5$NbOSi$_2$: C, 50.6; H, 7.1; N, 10.9. Found: C, 50.3; H, 7.0; N, 10.8.

Ta(N^{t}Bu){MeC(2-C$_5$H$_4$N)(CH$_2$NSiMe$_3$)(CH$_2$NC(OSiMe$_3$)-NTol)}Cl (18). To a stirred solution of [Ta(N^{t}Bu)(N$_2$N$_{py}$)Cl(py)] (230 mg, 0.341 mmol) in CH$_2$Cl$_2$ (20 mL) was added *p*-tolyl isocyanate (43 μL, 0.341 mmol). After stirring for 23 h at room temperature the volatiles were removed under reduced pressure to afford a yellow powder. Crystallization from CH$_2$Cl$_2$/hexanes at −30 °C afforded **18** as a pale yellow powder. Yield: 120 mg (48%). ^{1}H NMR (CD$_2$Cl$_2$, 500.0 MHz, 293 K): 9.36 (1 H, d, H^6, ^3J(H^{5}H^6) = 5.4 Hz), 7.83 (1 H, m, H^4), 7.52 (1 H, d, H^3, ^3J(H^{3}H^4) = 8.3 Hz), 7.29 (1 H, m, H^5), 7.05 (4 H, m, NC$_6$*H*$_4$Me), 3.60 (1 H, d, C*H*HNSiMe$_3$, ^2J = 13.7 Hz), 3.47 (1 H, d, C*H*HNCOSiMe$_3$, ^2J = 11.7 Hz), 3.30 (1 H, d, CH*H*NSiMe$_3$, ^2J = 13.7), 3.02 (1 H, d, CH*H*NCOSiMe$_3$, ^2J = 11.7 Hz), 2.25 (3 H, s, NC$_6$H$_4$*Me*), 1.46 (3 H, s, *Me*C(CH$_2$N)$_2$), 1.09 (9 H, s, CMe$_3$), 0.33 (9 H, s, NSiMe$_3$), −0.28 (9 H, s, OSiMe$_3$) ppm. ^{13}C{^{1}H} NMR (CD$_2$Cl$_2$, 125.7 MHz, 293 K): 163.5 (C^2), 155.7 (CO), 150.3 (C^6), 143.5 (*p*-C$_6$H$_4$Me), 139.2 (C^4), 131.4 (*i*-C$_6$H$_4$Me), 129.3 (*m*-C$_6$H$_4$Me), 123.2 (*o*-C$_6$H$_4$Me), 122.5 (C^5), 121.1 (C^3), 66.8 (*C*Me$_3$), 63.3 (CH$_2$NSiMe$_3$), 53.2 (CH$_2$NCOSiMe$_3$), 51.2 (Me*C*(CH$_2$N)$_2$), 31.8 (C*Me*$_3$), 22.9 (*Me*C(CH$_2$N)$_2$), 20.9 (C$_6$H$_4$*Me*), 2.1 (NSiMe$_3$), 0.1 (OSiMe$_3$) ppm. IR (KBr pellet): 3316 (w), 3109 (w), 3072 (w), 2968 (s), 2921 (m), 2894 (m), 2854 (m), 2752 (w), 2655 (w), 2592 (w), 2332 (w), 2161 (w), 2095 (w), 2002 (w), 1968 (w), 1923 (w), 1891 (w), 1868 (w), 1830 (w),

1792 (w), 1772 (w), 1749 (w), 1733 (w), 1716 (w), 1696 (w), 1684 (w), 1652 (w), 1636 (w), 1601 (s), 1572 (m), 1558 (w), 1510 (s), 1505 (s), 1468 (s), 1447 (m), 1438 (m), 1407 (m), 1379 (w), 1356 (m), 1333 (m), 1312 (w), 1284 (s), 1245 (s), 1216 (m), 1179 (w), 1165 (w), 1141 (w), 1122 (s), 1089 (m), 1061 (s), 1053 (s), 1023 (s), 1012 (m), 972 (m), 926 (s), 879 (m), 844 (s), 790 (w), 761 (m), 754 (m), 739 (w), 688 (w), 666 (m), 642 (w), 622 (w), 592 (w), 572 (m), 555 (w), 549 (w), 529 (w), 515 (w) cm^{-1}. EI mass spectrum: $m/z = 624$ (5%) $[M - Me]^+$. Anal. Calcd for $C_{27}H_{45}ClN_5OSi_2Ta$: C, 44.5; H, 6.2; N, 9.6. Found: C, 44.6; H, 6.2; N, 9.6.

Reactions of M(N^{t}Bu)(N$_2$N$_{py}$)Cl(py) (M = Nb, Ta) with CO$_2$. A solution of M(N^{t}Bu)(N$_2$N$_{py}$)Cl(py) (0.03 mmol) in CD_2Cl_2 (0.6 mL) was transferred to a J. Young NMR tube. The solution was degassed by three freeze−pump−thaw cycles before adding CO_2 (1 atm). The NMR tube was sealed and the reaction analyzed by NMR spectroscopy, which revealed a complex mixture of products.

Kinetic Analysis of SiMe$_3$ Migration in [W(NPh){MeC(2-C$_5$H$_4$N)(CH$_2$NSiMe$_3$)(CH$_2$N(SiMe$_3$)C(NAr)O}Me][MeBAr$^F_3$] (11-MeBAr$^F_3$). To [W(NPh)(N$_2$N$_{py}$)Me][MeBAr$^F_3$] (**2**) generated in situ in CD_2Cl_2 (0.6 mL) from W(NPh)(N$_2$N$_{py}$)Me$_2$ **1** (17.5 mg, 0.03 mmol) and BAr$^F_3$ (14.5 mg, 0.03 mmol) in the presence of 1,4-dimethoxybenzene (5.2 mg, internal standard) was added 2,6-diisopropylphenyl isocyanate (6.1 μL, 0.03 mmol). The mixture was transferred to a J. Young NMR tube and then to an NMR spectrometer probe that had been preheated to the desired temperature (one of 6 temperatures between 20 and 45 °C). After thermal equilibration ^{1}H NMR spectra were recorded every 5 or 10 min for a period of up to 4 h. First-order rate contants were obtained from linear plots of $-\ln(I/I_0)$ (I = pyridyl H^6 intensity for **11**$^+$ at a reaction time t; I_0 = estimated pyridyl H^6 intensity for **11**$^+$ at $t = 0$) vs t.

Re-evaluation of the Reaction of Ti(N^{t}Bu)(N$_2$N$_{py}$)(py) with ArNCO. To a solution of Ti(N^{t}Bu)(N$_2$N$_{py}$)(py) (21 mg, 0.04 mmol) in C_6D_6 (0.6 mL) was added 2,6-diisopropylphenyl isocyanate (9 μL, 0.04 mmol) and the reaction product Ti(N^{t}Bu){MeC(2-C$_5$H$_4$N)(CH$_2$NSiMe$_3$)(CH$_2$NC{N(SiMe$_3$)Ar}O}(py) (**20b**) analyzed by NMR spectroscopy (the chemical shift data were consistent with those previously reported[19]). ^{1}H NMR (C_6D_6, 300.1 MHz, 298 K): 9.66 (1 H, d, H^6, ^3J(H^{5}H^6) = 6.4 Hz), 9.35 (2 H, d, *o*-NC$_5$H$_5$, ^3J(H^{5}H^6) = 4.3 Hz), 7.07 (1 H, apparent td, H^4, ^3J(H^{4}H^5) = 8.0 Hz, ^3J(H^{4}H^3) = 8.0 Hz, ^4J(H^{4}H^6) = 1.9 Hz), 7.01 (1 H, d, *p*-C$_6H_3$^{i}Pr$_2$, ^3J = 7.6 Hz), 6.98 (1 H, m, *p*-C$_5$H$_5$N), 6.94−6.83 (3 H, overlapping m, *m*-C$_6H_3$^{i}Pr$_2$ and H^3), 6.74 (2 H, t, *m*-C$_5$H$_5$N, ^3J(H^{6}H^5) = 6.3 Hz), 6.69 (1 H, m, H^5), 3.72 (1 H, d, C*H*HC(NAr)OSiMe$_3$, ^2J = 12.9 Hz), 3.33 (1 H, d, CH*H*C(NAr)OSiMe$_3$, ^2J = 12.9 Hz), 2.77 (1 H, q, C*H*Me$_2$, ^3J = 6.8 Hz), 2.67 (1 H, q, C*H*Me$_2$, ^3J = 6.9 Hz), 2.31 (1 H, d, C*H*HNSi, ^2J = 12.9 Hz), 2.21 (1 H, d, CH*H*NSi, ^2J = 12.0 Hz), 1.58 (9 H, s, CMe$_3$), 0.98 (3 H, d, CH*Me*Me, ^3J = 6.9 Hz), 0.82 (3 H, d, CHMe*Me*, ^3J = 6.9 Hz), 0.78 (3 H, s, *Me*CCH$_2$), 0.69 (3 H, d, CHMe*Me*, ^3J = 6.8 Hz), 0.45 (3 H, d, CH*Me*Me, ^3J = 6.7 Hz), 0.40 (18 H, s, 2 × Si*Me*$_3$) ppm. ^{13}C{^{1}H} NMR (C_6D_6, 75.5 MHz, 298 K): 167.1 (*C*(NAr)OSiMe$_3$), 163.2 (C^2), 151.8 (C^6), 151.7 (*o*-NC$_5$H$_5$), 146.9 (*o*-C$_6$H$_3$^{i}Pr$_2$), 145.7 (*o*-C$_6$H$_3$^{i}Pr$_2$), 137.4 (*ipso*-C$_6$H$_3$^{i}Pr$_2$), 136.9 (*p*-NC$_5$H$_5$), 136.8 (C^4), 127.1 (*p*-C$_6$H$_3$^{i}Pr$_2$), 124.2 (C^3), 123.3 (*m*-NC$_5$H$_5$), 123.0 (*m*-C$_6$H$_3$^{i}Pr$_2$), 122.1 (*m*-C$_6$H$_3$^{i}Pr$_2$), 119.8 (C^5), 64.6 (N*C*Me$_3$), 64.4 (*C*H$_2$(NAr)OSiMe$_3$), 56.3 (*C*H$_2$NSiMe$_3$), 49.1 (Me*C*CH$_2$NSiMe$_3$), 33.5 (NC*Me*$_3$), 28.4 (overlapping 2 × *C*HMe$_2$), 25.1 (CH*Me*Me), 24.0 (CHMe*Me*), 23.7 (CHMe*Me*), 23.6 (CH*Me*Me), 22.1 (*Me*CCH$_2$), 3.1 (Si*Me*$_3$), 1.9 (Si*Me*$_3$) ppm.

Crystal Structure Determination of Nb(N^{t}Bu){MeC(2-C$_5$H$_4$N)(CH$_2$NSiMe$_3$)(CH$_2$NC(OSiMe$_3$)N^{t}Bu)}Cl (15). Crystal data collection and processing parameters are given in Table 6. Crystals of **15** were grown by slow evaporation of a pentane solution. A single crystal having dimensions of approximately 0.08 × 0.20 × 0.30 mm was mounted on a glass fiber using perfluoropolyether oil and cooled rapidly to 150 K in a stream of cold N_2 using an Oxford Cryosystems CRYOSTREAM unit. Diffraction data were measured using an Enraf-Nonius KappaCCD diffractometer. Intensity data were processed using the DENZO-SMN package.[45] The structure was solved in the space group $P2_1/n$ using the direct-methods program SIR92,[46] which located all non-hydrogen atoms for the four crystallographically independent molecules of **15** in the asymmetric unit. Subsequent full-matrix least-squares refinement was carried out using the CRYSTALS program suite.[47] Coordinates and anisotropic thermal parameters of all non-hydrogen atoms were refined. Hydrogen atoms were positioned geometrically after each cycle of refinement. A three-term Chebychev polynomial weighting scheme was applied. The crystal was of poor quality, causing considerable expansion of the diffraction peaks. This together with the relatively long *c* axis resulted in a substantial degree of peak overlap. Rejection of the overlapping peaks is responsible for the relatively poor completeness of the data set. It should be noted that there are still over 10 observed independent measurements per refined parameter. The thermal parameters of some of the *tert*-butyl and trimethylsilyl C atoms were relatively large. However, attempts to model these groups as disordered did not significantly improve the agreement with the X-ray data so were abandoned.

Table 6. X-ray Data Collection and Processing Parameters for Nb(N^{t}Bu){MeC(2-C$_5$H$_4$N)(CH$_2$NSiMe$_3$)-(CH$_2$NC(OSiMe$_3$)N^{t}Bu)}Cl (15)

empirical formula	$C_{20}H_{41}N_4Si_2Ta$
fw	606.21
temp/K	150
wavelength/Å	0.71073
space group	$P2_1/n$
a/Å	16.8425(3)
b/Å	21.5100(4)
c/Å	36.4135(7)
α/deg	90
β/deg	100.7414(6)
γ/deg	90
V/Å^3	12960.8
Z	16
d(calcd)/Mg·m^{-3}	1.243
abs coeff/mm^{-1}	0.551
R indices R_1, R_w [$I > 3\sigma(I)$][a]	$R_1 = 0.0433$, $R_w = 0.0501$

[a] $R_1 = \Sigma||F_o| - |F_c||/\Sigma|F_o|$; $R_w = \{\Sigma w(|F_o| - |F_c|)^2/\Sigma(w|F_o|^2\}^{-1/2}$.

A full listing of atomic coordinates, bond lengths and angles, and displacement parameters for **15** have been deposited at the Cambridge Crystallographic Data Center. See Notice to Authors, Issue No. 1.

Computational Details. All calculations were performed with the Gaussian98 set of programs[48] within the framework of hybrid DFT (B3PW91)[49,50] and ONIOM(B3PW91/UFF),[51]

(45) Otwinowski, Z.; Minor, W. *Processing of X-ray Diffraction Data Collected in Oscillation Mode, Methods in Enzymology*; Academic Press: New York, 1997.

(46) Altomare, A.; Cascarano, G.; Giacovazzo, G.; Guagliardi, A.; Burla, M. C.; Polidori, G.; Camalli, M. *J. Appl. Crystallogr.* **1994**, *27*, 435.

(47) Watkin, D. J.; Prout, C. K.; Carruthers, J. R.; Betteridge, P. W.; Cooper, R. I. *CRYSTALS, issue 11*; Chemical Crystallography Laboratory: Oxford, UK, 2001.

(48) Frisch, M. J.; Trucks, G. W.; Schlegel, H. B.; Scuseria, G. E.; Robb, M. A.; Cheeseman, J. R.; Zakrzewski, V. G.; Montgomery, J. J. A.; Stratmann, R. E.; Burant, J. C.; Dapprich, S.; Millam, J. M.; Daniels, A. D.; Kudin, K. N.; Strain, M. C.; Farkas, O.; Tomasi, J.; Barone, V.; Cossi, M.; Cammi, R.; Mennucci, B.; Pomelli, C.; Adamo, C.; Clifford, S.; Ochterski, J.; Petersson, G. A.; Ayala, P. Y.; Cui, Q.; Morokuma, K.; Malick, D. K.; Rabuck, A. D.; Raghavachari, K.; Foresman, J. B.; Cioslowski, J.; Ortiz, J. V.; Baboul, A. G.; Stefanov, B. B.; Liu, G.; Liashenko, A.; Piskorz, Y.; Nanayakkara, A.; Gonzalez, C.; Challacombe, M.; Gill, P. M. W.; Johnson, B.; Chen, W.; Wong, M. W.; Andres, J. L.; Head-Gordon, M.; Replogle, E. S.; Pople, J. A. *Gaussian 98, Revision A.11*; 2001.

(49) Becke, A. D. J. *Chem. Phys.* **1993**, *98*, 5648.

(50) Perdew, J. P.; Wang, B. *Phys. Rev. B* **1992**, *45*, 13244.

where the QM part was treated at the B3PW91 level and the MM calculations were performed with the Universal Force Field (UFF) of Rappé et al.[52] In the DFT calculations the ligand N_2N_{py} has been modeled by $HC(2\text{-}C_5H_4N)(CH_2NSiH_3)_2$ (abbreviated as N_2N_{qm}), and the missing Me groups have been treated at the MM level (UFF) in the ONIOM calculations. The QM part of the ONIOM calculations is the same as that for the DFT-only calculations. CO_2 has been explicitly treated at the DFT level in all calculations. The isocyanate RNCO are modeled by MeNCO in the DFT calculations and by ^{t}BuNCO in the ONIOM calculations, where the three methyl groups on the *tert*-butyl are treated at the UFF level. In all calculations, the metal atom (W, Ta)[53] and Si[54] have been treated with effective core pseudo-potentials from Dolg's group and the associated basis sets, augmented by polarization functions.[55,56] The atoms directly bonded to the metal (N and CH_3) as well as CO_2 and the NCO atoms in RNCO were treated with a 6-31G(d,p) basis set.[57] All the other atoms were represented with 6-31G basis sets in the calculations.[58] Geometry optimizations were performed without any symmetry constraint and were followed by analytical calculations of the Hessian matrix to check the nature (minimum or transition state) of the located extrema. Connection between two local minima through a particular TS was checked by slightly altering the TS geometry along the TS vector in both directions followed by optimization as a local minimum of the resulting guess geometries. The NBO procedure[44] used was that implemented in Gaussian98. Gibbs free energy values were obtained from the frequency calculations with Gaussian98 and are given at $T = 298$ K unless otherwise stated.

Acknowledgment. We thank the EPSRC, Leverhulme Trust, and Royal Society (P.M.), British Council (P.M., L.H.G. and E.C.), the CNRS (E.C.), and the DFG (L.H.G.). E.C. and P.M. thank the Royal Society of Chemistry for financial support (International Authors Travelling Grant). We acknowledge the use of the EPSRC National Service for Computational Chemistry Software and the UK Computational Chemistry Facilty.

Supporting Information Available: X-ray crystallographic file in CIF format for the structure determination of $[Nb(N^tBu)\{MeC(2\text{-}C_5H_4N)(CH_2NSiMe_3)(CH_2NC(OSiMe_3)N^tBu)\}Cl]$ (**15**); rate plots for the conversion of $\mathbf{11}^+$ to $\mathbf{12}^+$ and further details of the DFT-computed distances and angles. This material is available free of charge via the Internet at http://pubs.acs.org.

OM0500265

(51) Svensson, M.; Humbel, S.; Froese, R. D. J.; Matsubara, T.; Sieber, S.; Morokuma, K. *J. Phys. Chem.* **1996**, *100*, 19357.
(52) Rappe, A. K.; Casewit, C. J.; Colwell, K. S.; Goddard, W. A.; Skiff, W. M. *J. Am. Chem. Soc.* **1992**, *114*, 10024.
(53) Andrae, D.; Häusserman, U.; Dolg, M.; Stoll, H.; Preuss, H. *Theor. Chim. Acta* **1990**, *77*, 123.
(54) Bergner, A.; Dolg, M.; Chle, W. K.; Stoll, H.; Preuss, H. *Mol. Phys.* **1990**, *30*, 1431.
(55) Ehlers, A. W.; Böhme, M.; Dapprich, S.; Gobbi, A.; Höllwarth, A.; Jonas, V.; Köhler, K. F.; Stegmann, R.; Veldkamp, A.; Frenking, G. *Chem. Phys. Lett.* **1993**, *208*, 111.
(56) Höllwarth, A.; Böhme, M.; Dapprich, S.; Ehlers, A. W.; Gobbi, A.; Jonas, V.; Köhler, K. F.; Stegmann, R.; Veldkamp, A.; Frenking, G. *Chem. Phys. Lett.* **1993**, *203*, 237.
(57) Hariharan, P. C.; Pople, J. A. *Theor. Chim. Acta* **1973**, *28*, 213.
(58) Hehre, W. J.; Ditchfield, R.; Pople, J. A. *J. Chem. Phys.* **1972**, *56*, 2257.